EFFECT OF TANTALUM ON BORON FREE AND BORON DOPED INTERMETALLIC COMPOUND Ni Al

A Thesis Submitted
In Partial Fulfilment of the Requirements
for the Degree of
MASTER OF TECHNOLOGY

by

AMIT SINGHAL

to the

DEPARTMENT OF METALLURGICAL ENGINEERING
INDIAN INSTITUTE OF TECHNOLOGY, KANPUR

AUGUST, 1989

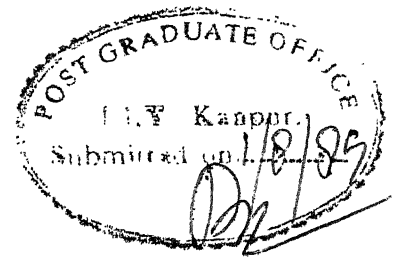

CERTIFICATE

This is to certify that the work on "EFFECT OF Ta ON BORON FREE AND BORON DOPED INTERMETALLIC COMPOUND NiAl" has been carried out by Mr. Amit Singhal under my supervision and it has not been submitted elsewhere for a degree.

August, 1989.

(A.K. Jena)
Professor
Department of Metallurgical Engineering
Indian Institute of Technology
Kanpur

ME-1989-M-SIN-EFF

ACKNOWLEDGEMENTS

Working with Professor A.K. Jena has been a very good and memorable experience. I feel myself previleged to have been able to work with him. With his excellent guidance and constant advice, he has made this work very interesting and I esteem very much the valuable experience, I gained under his supervision.

It gives me great pleasure to thank my colleagues. I would like to acknowledge specially the help I got from Mr. V. Kumar. I would also like to thank Mr. I. Mukherjee, Dr. H.K. Gupta, Mr.R.R. Nagrajan and Ms. Archna Gupta for their valuable assistance at various stages of the work. I am also thankful to Mr. G.S. Thapa for drawing the figures in this thesis.

The pain and immense care that Mr. U.S. Misra took in typing the manuscript in a very short time is gratefully acknowledged.

Amit Singhal

-Amit Singhal

CONTENTS

LIST OF TABLES

LIST OF FIGURES

ABSTRACT

In the present investigation, effect of Ta and B on NiAl phase has been studied. The phase stability study has been made at two different temperatures 1200°C and 1000°C. In the present work, X-ray diffraction and microstructural study has been done to identify the extra phases present in alloys as well as to measure the lattice parameter of NiAl phase. Compression testing was also done to have an idea of effect of Ta and B on the strength and ductility of β -phase. Lattice parameters of NiAl decreases with increasing addition of Ta, while presence of B causes slight increase in the lattice parameter. Solubility of Ta in NiAl is very small when nickel is constant at 50%. The solubility loop is not symmetric. Suggesting that Ta has tendency to substitute to Ni and aluminium rather than aluminium alone. Boron does not have any effect on the solubility of Ta in NiAl. Ta increases the 0.2% proof stress of NiAl phase. In presence of Ta and Boron, strength of NiAl phase increases by about 200% while the ductility remains high. Ta and boron increases the hardness of NiAl. Some of the alloys show small percentage of a precipitating phase on the grain boundaries. It was recognised as TaC. Solubility of TaC decreases appreciably with decrease in temperature.

CHAPTER 1

INTRODUCTION

Intermetallic compounds have considerable promise for high temperature applications. They are expected to be better then the Ni-base super alloys which have been traditionally used at high temperature. Intermetallic compounds of nickel-aluminium system are of special interest. Ni_3Al and NiAl are the best intermetallic compounds in the nickel-aluminium system. Ni_3Al has unique mechanical properties flow stress increases with temperature upto about 600^{o}-$700^{o}C$. Because of this property Ni_3Al becomes an ideal material for high temperature applications. It is the intermetallic compound which is being used as a second phase in Ni-base super alloys. Intermetallic compound NiAl has better oxidation resistance ($1095^{o}C$) and corrosion resistance than Ni_3Al. Therefore it could proved to be an asset for high temperature applications.

Future improvements of the jet engine performance will require materials which are lower in density and can withstand higher temperature thus increasing the thrust to weight ratio and engine efficiency. The intermetallic compound β-NiAl is a prime candidate for this new high temperature materials. This intermetallic compound offers a low density, a high melting temperature, excellent

oxidation resistance and very good corrosion resistance. Order intermetallics have long been recognized as candidates for higher temperature applications because thermally activated process such as diffusion are inhibited by the ordered, crystal structure. The ordered intermetallic NiAl is especially attractive since this compound remains ordered up to its high congruent melting point of 1640°C, and has an ordered structure over a range of compositions.

The draw backs of NiAl, however, are its room temperature brittleness and its inadequate creep resistance at high temperature inspite of its ordered crystal structure. Creep properties can be enhanced by solute additions. The mechanical properties of intermetallics compounds are systematically affected by phase stability which can be varied by ternary additions. For example, addition of Ti and Zr cause severe lattice distortion with a consequent improvement in strength and stress to rupture characteristics. The NiAl + 4 percent Zr alloy retains a transverse rupture strength 11-20 kg/mm^2 up to 1100°C, whereas unalloyed NiAl ruptures at 4-355 kg/mm^2 under these conditions.

In the present investigation effect of Ta and B on the phase stability of NiAl has been studied by X-ray diffraction studies, microhardness measurements, microstructural observations and high temperature compression test.

CHAPTER 2

LITERATURE REVIEW

2.1 Introduction

Superalloys are generally used at temperatures of 650°C and above where relatively severe mechanical stressing is encountered and where surface stability is often required.

Superalloys are divided into three classes, nickel base super alloys, cobalt base super alloys and iron base super alloys. The term super alloys can also be applied to complex combinations of iron, nickel, cobalt and chromium. These alloys consist of various amounts of iron, nickel, cobalt and chromium as well as minor amounts of tungsten, molybedum, tantalum, niobium, titanium and aluminium.

Superalloys because of their retention of strength at high temperature are utilized at a higher proportion of their actual melting point. Superalloys are used in gas turbine, aircraft industries, space vehicles, rocket engines and for other higher temperature components.

Ni-base superalloy are widely used at high temperatu in wrought conditions. Ni-base superalloys (1) are both solid solution and precipitation strengthened. Most of Ni-base alloys (2) contain 10 to 20% Cr, upto 8% Al and Ti, 5-10% Co and small amount of boron, Zr and C.

The alloying elements can be grouped with some commonality in the periodic system. The first class consists of elements stabilize the face-centered cubic austenite (γ) matrix. These are from groups V, VI and VII and include nickel, cobalt, iron, chromium, molybdenum and tungsten. The second class of elements partition to make up the γ' precipitate Ni_3X. These elements are from groups III, IV and V and include Al, Ti, Cb, Ta and Hf.

Solid solution strengthened alloys (1) have been used widely in burner and combustor applications in gas turbine engines. It exhibits high temperature corrosion/errosion resistance combined with excellent fabricability and weldability. The precipitation-strengthened alloys are selected for high temperature strength. These alloys which are strengthened by secondary precipitated phase are the most remarkable of all the superalloys. These alloys exhibit a face centered cubic (fcc) austenite solid solution matrix or back ground metal with a nickel-aluminium-titanium compound (known as γ') as the principal strengthening phase.

Various carbides depending on the particular alloy composition and heat treatment also exist as secondary precipitated phases. The γ'-strengthened nickel superalloys are used in the most demanding applications relative

to stress and temperature in gas turbines engines. Another strengthening mechanism in nickel alloys in the presence of dispersed oxide particles in the structure. Such dispersion strengthened alloys exhibit the highest strength at the most elevated temperatures, but only low-to-moderate strength at intermediate temperature.

The intermetallic compounds which are likely to be better than the superalloys may be expected to be found in the Ni-Al-X systems where X in this investigation has been taken as Ta.

2.2 Ni-Al System

Hansen and Anderko (3) gave the Ni-Al binary systems. The diagram is represented in Figure 2.1. The partial phase diagram for alloys with 0-50 atm. Ni is well established.

There are two intermediate particularly formed phases:

$NiAl_3$ (42.03 wt% Ni) is formed particularly at 854^{o}C and the other intermediate phase forms particularly at 1132-1133^{o}C and was in finally accepted to be of ideal composition (59.19 wt% Ni). The γ' phase based on the stochiometric composition has a maximum melting point of 1638^{o}C.

The constitution in the 50at% - 100 at% Ni proved to be more complicated. Ni_3Al according to Hausen and Anderko (3) has and ordered fcc structure, NiAl has ordered bcc structure and Ni_2Al_3 is hexagonal $D0_{19}$ type.

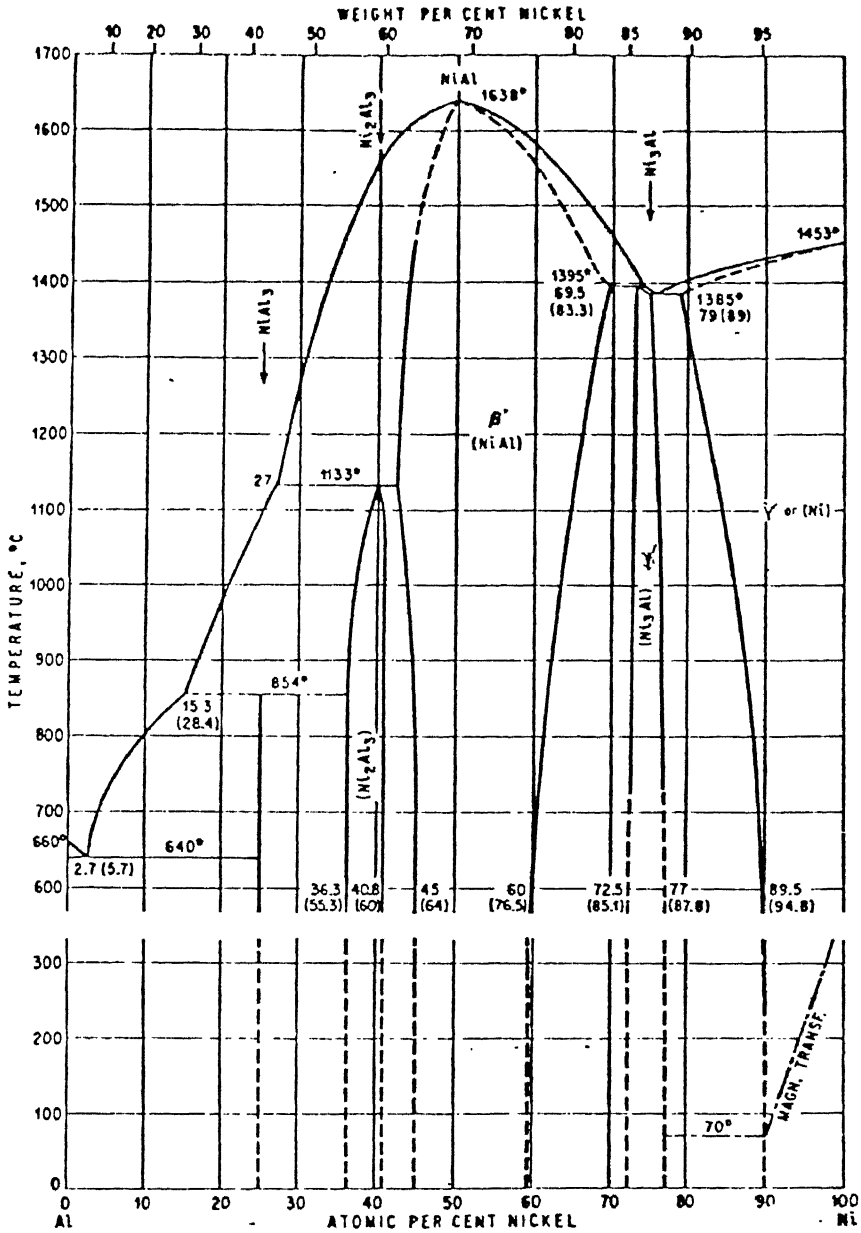

Fig 2.1: Binary phase diagram of Ni-Al

According to M.J. Copper (4) lattice parameter of NiAl at 50.76 at%Al is maximum and it is equal to $2.8864 \pm .0006 A^{o}$. According to Hausen and Anderko (3) at room temperature NiAl exists from 45at% Ni to 60at% Ni.

Electrical resistivity and thermal dilation measurement exhibit sharp minima at the compositions NiAl and Ni_3Al at constant temperature (3).

2.3 Ni-Ta System

Hansen and Anderko (3) gave the phase diagram for Ni-Ta system. It is shown in Fig. (2.2). Later it was modified by Shunk (5) which is modified by Nash and West (6) and confirmed the existence at $1320^{o}C$ (1593 K) which was first reported by Larsen et al (7). It was found that Ni_3Ta is a long range ordered stochiometric compound with fct structure, isomorphous with $NbNi_8$.

Ni_3Ta was first discovered by Therkelsen (8). There are three distinct structural modification of Ni_3Ta have been reported. One found is orthorhombic of the structure type $TiCu_3$ and second found is tetragonal $TiAl_3$ (DO_{22})-type structure. Third found which is the equilibrium form of Ni_3Ta. They identified the crystal structure as monoclinic of type $TaPt_3$.

NiTa was obtained at 50.0 at% Ta formed a peritectic reaction at $1570^{o}C$. The structure of NiTa was found to be of

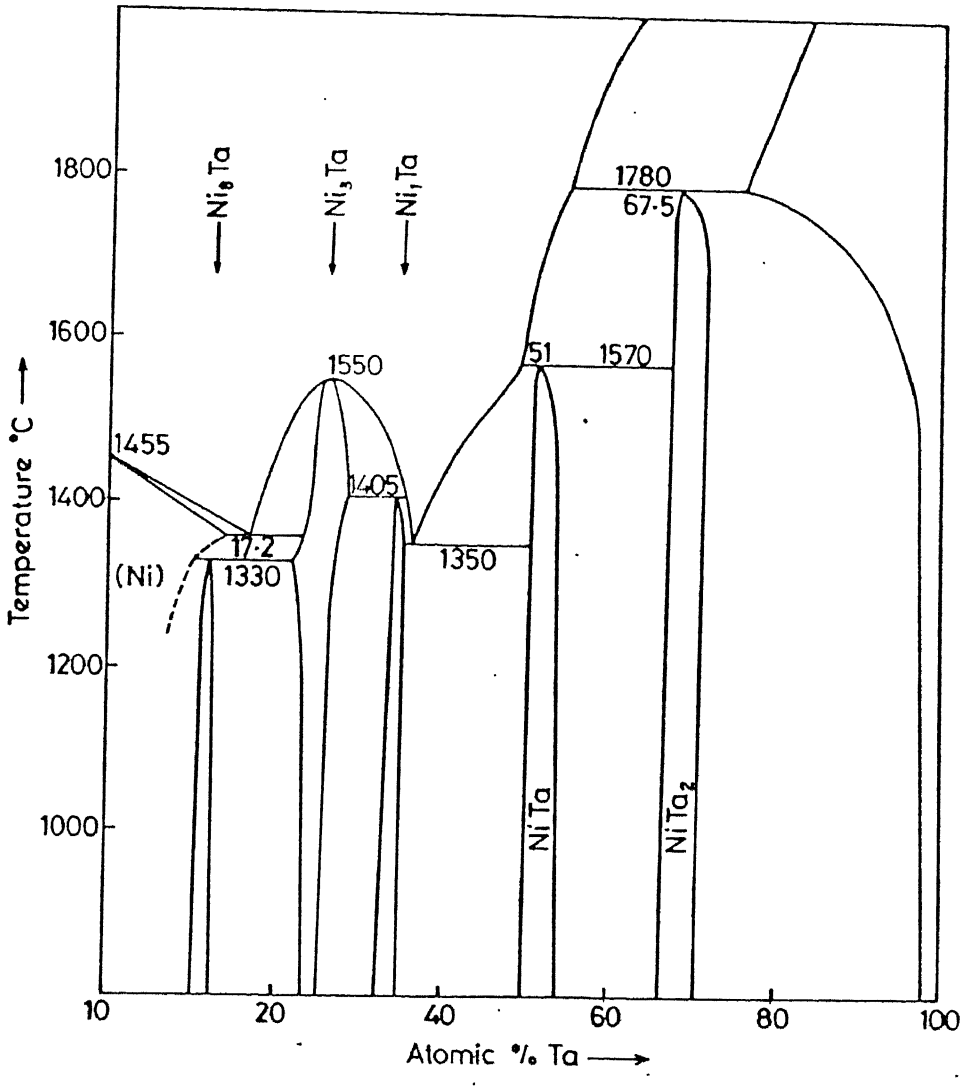

Fig 2.2: Binary phase diagram of Ni-Ta

W_6Fe_7 type with lattice parameter a = 0.4921 mm and C = 2.6905 mm.

Ni_2Ta has a tetragonal structure and found peritectic alloy at 1420°C at 33.3 at% Ta (9).

Ni_2Ta has been reported (9) to formed at 1788°C found a peritectic reaction. It has bet structure with lattice parameters, a = 0.6216 mm, C = 0.4872 mm.

2.4 Al-Ta System

Hansen and Anderko (3) reported that existence of the compound. $TaAl_3$ (69.09 wt% Ta). Its structure is said to be DO_{22} with the lattice parameter, a = 5.433 A°, C = 8.533 A° and c/a = 1.574.

Eliot (10) reported the existence of $TaAl_3$, $TaAl_2$ and a σ phase of wide homogenity 64.80%Ta. Eashmmer et al (11) gave the σ phase the nominal composition Ta_2Al. The σ phase said to be tetragonal (10) with lattice parameter a = 9.825 A°, c = 5.23 A°, at ~ 67 at% Ta and a = 9.98 A°, c = 5.16 A° at ~75 at% Ta. Shrunk (5) reported that $TaAl_3$ and Ta_2Al are formed peritectically. He also reported the existence of a high temperature phase $Ta_{17}Al_{12}$ which is a BCC, α-Mn type with a = 9.88 A°. A phase which tentatively indexed as cubic with a = 19.2A° having composition between $TaAl_2$ and $TaAl_3$ was also observed. Phase diagram is shown in Figure (2.3).

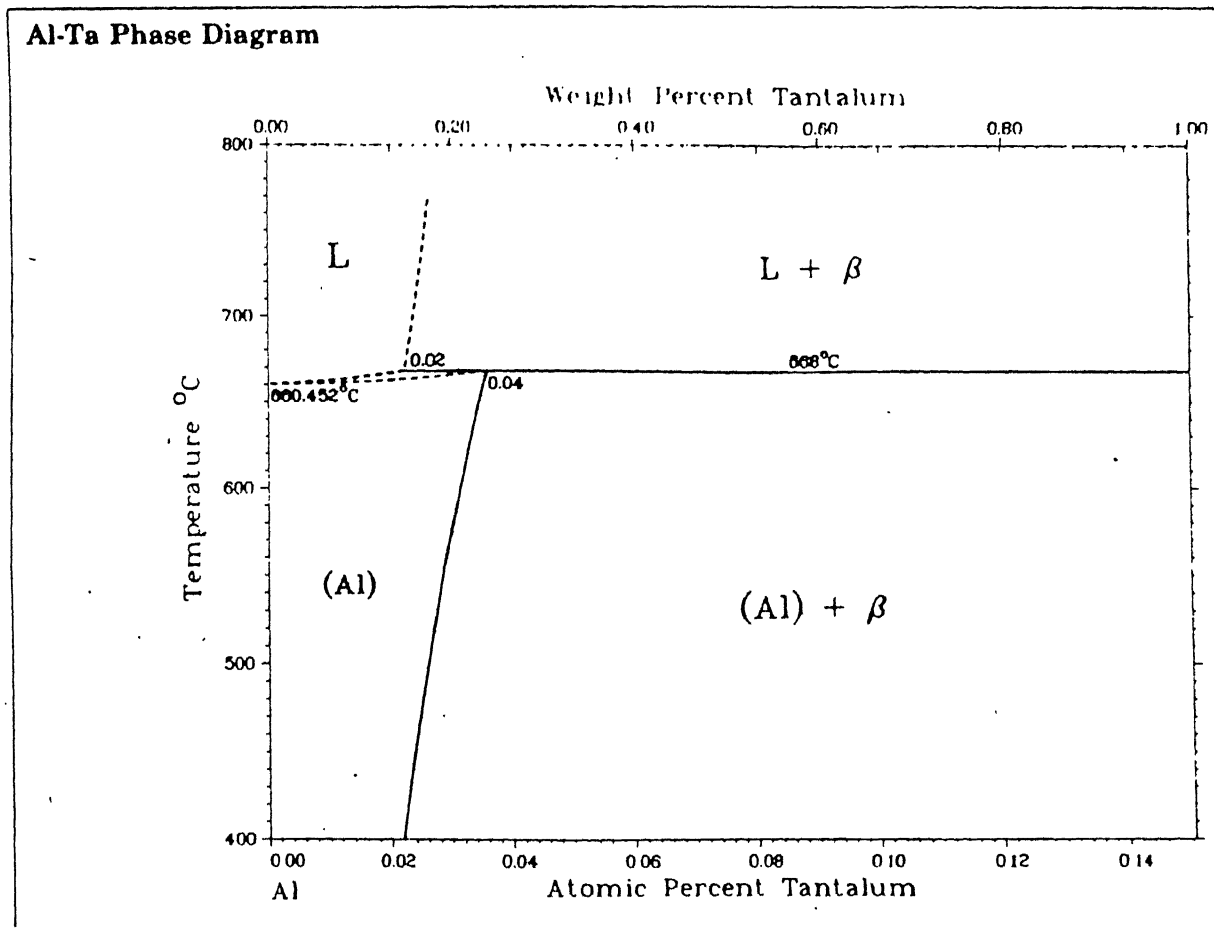

Fig 2.3: Binary phase diagram of Al-Ta

2.5 Ni-Al-Ta System

Inspite of the practical importance the Ni-Al-Ta system has been relatively investigated. According to Hansen and Anderko (3) eutectic and a peritectic reaction runs in the region of Ni_3Al. Nash and West (12) who studied solid state equilibria at 1573K and 1273K. Partial isothermal sections at 1573K and 1273K are showed in Fig. 2.4 and Fig. 2.5. They confirmed the existence of intermediate phase Ni_6Ta^{Al} (η). It has a range of solubility in the direction of constant tantalium/aluminium ratio but a more limited solubility range for constant nickel composition. They also reported that ternary intermediate phase H (based on Ni_2TaAl) enters into equilibrium with the phases, β , NiTaAl, μ and δ (Ni_3Ta). A peritectoid reaction was reported at a temperature range between 1273K and 1573K.

$$\beta\ (NiAl) + \mu\ (NiTa) \rightarrow NiTaAl + H(Ni_2TaAl).$$

Nash and West (12) reported that phase has very little tantalum solubility at the nickel rich end but the solubility increases to about 5 atomic % Ta when the $\beta + Ni_3Al + \eta$ equilibrium is reached at 1573K.

On decreasing the temperature to 1273K, the solubility of tantalum in β-phase decreases sharply. Shrunk (5) who gave Ni-Ta binary phase diagram is modified by Nash and West (12) and confirmed the existence of Ni_8Ta

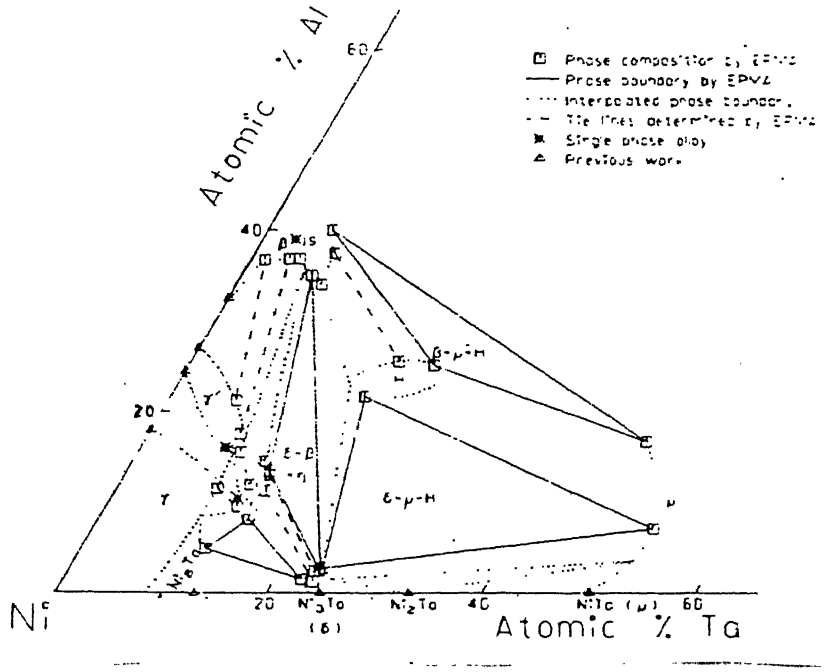

Fig 2.4: Isotherm of Ni-Al-Ta system at 1250 °C

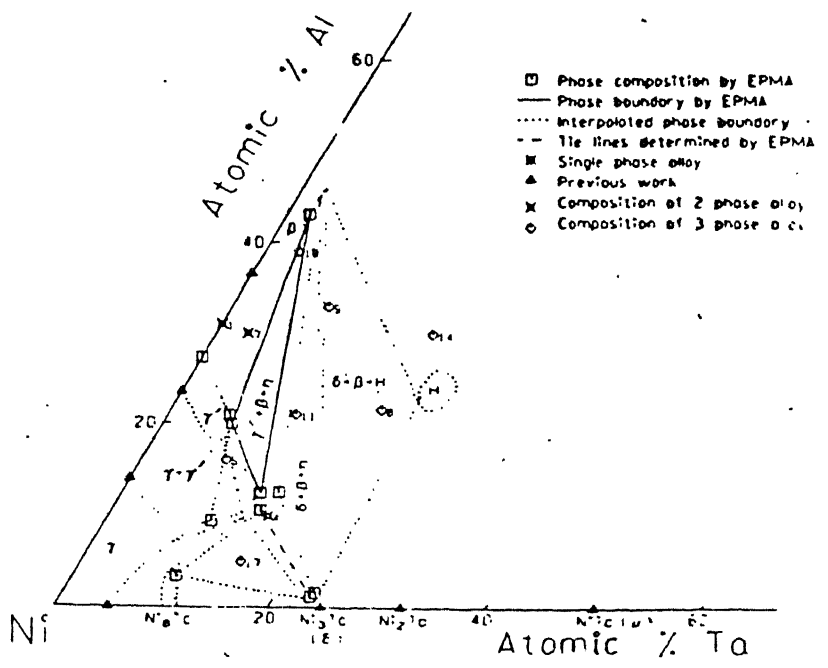

Fig 2.5 : Isotherm of Ni-Al-Ta system at 1000 °C

at 1593K which was first reported by Larsen et al (7) and note that a peritectoid reaction occur at high temperature and it was found to lie between 1593K and 1613K. Ni_8Ta has a face centered tetragonal structure, lattice parameter are a' = b' = 10.754 A^o and c'/a' ratio is greater than 10. It was reported by Larsen et al (7). According to Hubert et al (13) in a Ni-Al-Ta system, a pseudo binary eutectic between Ni_3Al (γ') and Ni_3Ta(δ) at 11.9 at% Ta and 12.6 at% occur and according to Hubert et al (13) a ternary eutectic between γ, γ' and δ at 11.0 at% Ta and 9.05 at% Al occur. Giessen and Grant (14) reported the existence of Ni_6TaAl in Ni_3Al (γ') and Ni_3Ta (δ) system which has been designated by η. This is also confirmed by Mint et al (15) and Nash and West (12). Mint et al (15) reported that melting point of Ni_6TaAl is 1530^oC (1803K). Structure of Ni_6TaAl phase is hexagonal and it is similar to Ni_3Ti. Ni_3Ta which has Ta solubility up to 25 at% 1573K possess an orthorombic structure identical with the Cu_3Ti structure it was reported by Karnilov (16). Ternary phase Ni_6TaAl shows extensive solid solubility for nickel.

Willemin et al (17) did a detail study of system (1 to 10) and early results on liquid solid transformation have already been published (18). According to Willemin et al (18) within the triangle Ni-NiAl-Ni_3Ta five phase exist γ,γ' ,δ ,β and Ni_6TaAl. Crystal structure and lattice parameter are given in Table (2.1) (17).

According to Willemin et al (18) solubility of Ta in NiAl(β) is very low 10-6at% while in γ , γ ',δ and Ni_8Ta it is very high. All these datas are given in Table 2.2 (17). Compound Ni_8Ta does not exist up to the solidus temperature. Willemin et al (17) determined the lines for the solid state equilibria by microprobe analysis for the 1250°C isothermal section. Several two phase fields made this part of the diagram, as show in Figure (2.6).

In Ni-Al-Ta system Al is considerably substituted by Ni and Ta with replacement of upto 60% of the Al atom.

TEM of a β -NiAl alloy containing a dispersion of submicron size second phase ppt in its matrix (19) At higher level of Ta at least three possible ternary compound are reported in literature.

NiAlTa has a hexagonal. $MgZn_2$ type structure (14) with a unit cell containing four molecular unit (20). Ni_2AlTa has the cubic Cu_2AlMn type structure with a = 0.5949 nm (15) $(Al_{0.5}\ Ta_{0.5})\ Ni_3$ has the hexagonal. Ni_3Ti type (DO_{24}) structure with a_o = 0.5112 nm and c_o = 0.8340 nm (21).

Vedula et al (22) calculated the lattice parameter of NiAlTa precipitate and they reported $a_o = 0.4903 \pm 0.0013$ n and $c_o = 0.7929 \pm .0029$ nm. Nash and West (12) reported a_o = .5015 nm and c_o = .8171 nm for NiAlTa precipitate in and alloy containing 59.3 at% Ni, 35.8 at% Al and 4.9 at% Ta.

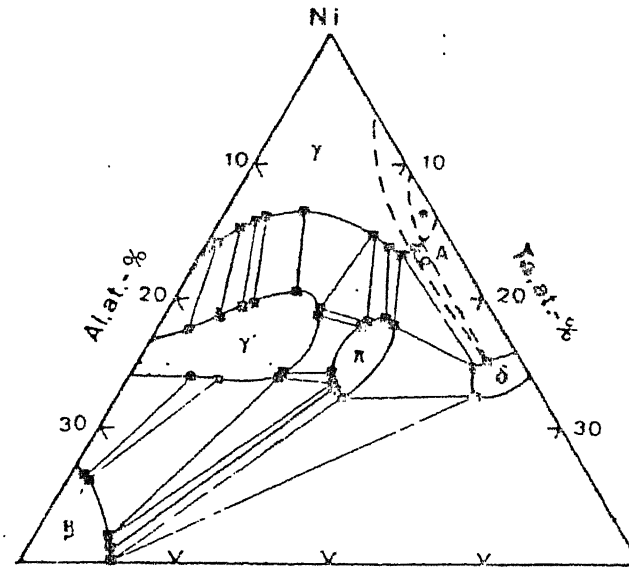

Fig 2.6: Isotherm of Ni-Al-Ta system at 1250 °C

Table 2.1 : Crystal Structure and Lattice Parameters (nm) A_2B Phases in Ni-Al-Ta System

Composition at% (Ni base)		Equivalent Ni Base Compound					
		Ni_3Al	Ni_6TaAl	Ni_3Ta	Ni_3Ta	Ni_3Ta	Ni_8Ta
		Phase type Cu_3Au	Ni_3Ti	Al_3Ti	Pt_3Nb	Cu_3Ti	Cu_3Ti
Al	Ta	Bravis lattice simple cubic	Hexagonal	BCT	Monoclinic	Ortho-rhombic	FCT
31.0	0	a=0.3573					
12.6	11.8	a=0.3607					
13.1	8.9	a=0.3608					
18.0	7	a=0.3609					
10.5	12		a=0.5114 c=0.8360				
10.4	14.3		a=0.5114 c=0.8362				
12.5	12.5		a=0.5112 c=0.8340				
12.5	12.5		a=0.5137 c=0.8366				
0	25			a=0.3627 c=0.7455	a=0.512 b=0.452 c=2.537, $\alpha = 90.50^{\circ}$,	a=0.512 b=0.423 c=0.452	
0	25				a=0.511 b=0.454 c=2.550, $\alpha = 90.38^{\circ}$,	a=0.5114 b=0.4250 c=0.4542	
2.5	26			a=0.3571 c=0.7452			
0	11.1					a=0.5117 b=0.4247 c=0.4527	
							a=1.0754 c=0.3585

Table 2.2 : Limiting Compositions of Phases, corresponding to Maximum Solubility for primary Phases (All except Ni_8Ta)

Phase	Composition at%		
	Al	Ta	Ni
	8-12	13.5-14.5	70-80
	0-2.5	23.5-25	70-85
	30-55	0-6	42-70
	7-25	0-10	75-80
	0-15	0-15	80-100
Ni_8Ta	0-4	12-14	84-88

The second phase precipitate in the β-NiAl + 2at% Ta alloy were identified by X-ray diffraction to be NiAlTa with a hexagonal C_{14} structure. The precipitate has a plate like shape.

2.6 Intermetallic Compound NiAl (Beta Phase)

2.6.1 Structure

NiAl is an ordered compound with the CsCl (B_2) structure and exists over a wide range of composition on both side of equiatomic composition at room temperature (3). Structure of NiAl is shown in Figure (2.7). Bradley and Taylor (23) found that density of NiAl alloy increased with increase in the Ni content but lattice parameter is maximum near the stoichiometric composition. Because on increasing the Ni-content, replacement of Al atoms by smaller Ni atoms occur. This results increase in density and decrease in lattice parameter. While on increase in aluminium content, aluminium atoms do not replace nickel atoms. So Ni ion vacancy occur due to which decrease in density as well as decrease in lattice parameter occur. Variation of lattice parameter of NiAl is shown in Fig. (2.8).

According to Copper (4) maximum lattice parameter occurred at 50.76±0.11 at% Al and density determined by displacement method was 5.85±0.06 gm/cm^3.

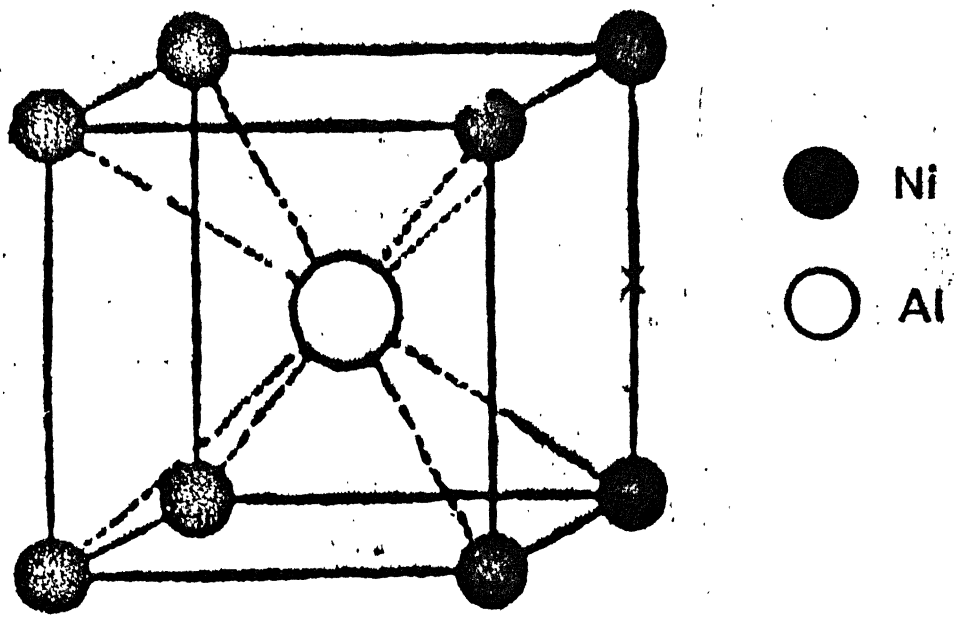

Fig 2.7 : Structure of NiAl phase

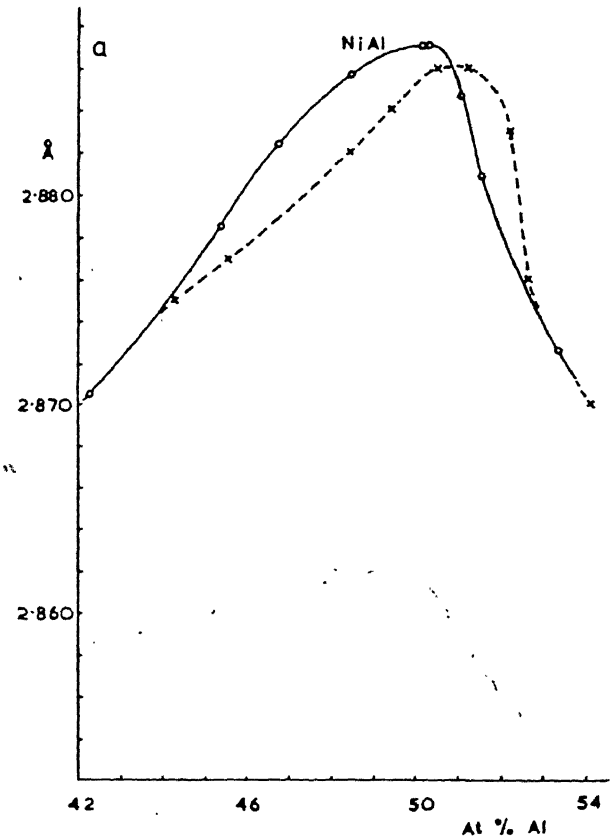

——○—— Bradley and Taylor (1937).
----×---- Guseva (1951).

Fig 2.8 : Variation of lattice parameter with composition for NiAl

Lattice parameter of intermetallic compound NiAl reported by several workers are given below:

(4)	M.J. Copper (1962)	$2.8864 \pm .00006\ A^{\circ}$
(23)	Bradley and Taylor (1937)	$2.8872 \pm .0002 A^{\circ}$
(24)	Guseva (1951)	$2.886 A^{\circ}$

The peak in lattice parameter occurs at 50.76at% Al, i.e. towards the aluminium rich side of ideal 50-50at% composition some replacement of nickel atoms by aluminium atoms must occur upto the maximum of about 1.5%.

2.6.2 Ordering

Ordering in CsCl type of structure is controlled by size and electron to unit cell ratio (25). In β-phase e/a is 1.5 according to Home Rothery's rule. This is achieved at composition of 50-50 at%. This corresponds to 3.0 electron per unit cell. This value is not to be exceeded when further Al is added. This is possible only when nickel atoms are replaced by vacancies not by aluminium atoms.

According to Bradley et al (23) electron/unit cell is a essential factor which decide at which composition vacancies formation occur and size factor is important in determining rate at which vacancies formation occur.

2.6.3 Diffusion in β -Phase

Intermetallic compound NiAl has become the one of the most important compound for high temperature properties for which diffusion plays a significant role in many processes which occur at temperature above 0.4 Tm. Diffusion behaviour of aluminium rich alloys are affected by composition. This was shown by Berkowitz et al (26). Hancok et al (27) showed that as the temperature decreases nickel self diffusion coefficient (D) decreases.On increasing the nickel content in nickel rich,NiAl at a particular temperature self diffusion coefficient of nickel increases while they did not find the same trend in aluminium rich. NiAl compound but the self diffusion coefficient of nickel is higher in high aluminium rich NiAl compound in comparison to low aluminium. NiAl compound variation of diffusion with composition is shown in Figure (2.9). They reported that diffusion coefficient is a minimum at an off stoichiometric composition (~ 49.5 at%Ni). Further there some evidence that the composition at which the minimum in D occurs is temperature dependent.

The most probable mechanism of diffusion in CsCl type alloys (28 to 30) is six jump cycle which allows diffusion to take place by means of neighbouring jumps. The first three jump move the atoms to wrong sites increasing

local disorder while last three jumps restore atoms to their correct sites. Elock et al (28) and Elock (29) predicted that for CsCl type intermetallic compound diffusivities of two elements A-B should be lie within the limits $3/2 \geq D_A/D_B \geq 2/3$ for the six jump cycle mechanism.

Hancock et al (27) predicted that diffusion mechanism in NiAl should be a six jump cycle but this may not be possible that is explained by two reasons. Firstly in most nearest jumps which unlike the six jump cycle involve no disordering are likely to be favoured in high order energy system. Secondly the presence of high vacancy concentration in aluminium rich alloys also favours next-nearest neighbour exchange.

Hancock et al (27) reported that activation energy Q. Steadily decreases with increase in nickel content in nickel rich side of stoichiometry. Presence of vacancies produces a drastic decrease in diffusion activation energy, this drastic change in activation energy shows that vacancy diffusion mechanism is operative in NiAl alloys. Variation of activation energy with composition is shown in Figure (2.10). Wasilewski (31) has considered the formation of structure defects in intermetallic compound NiAl. In this type of component at

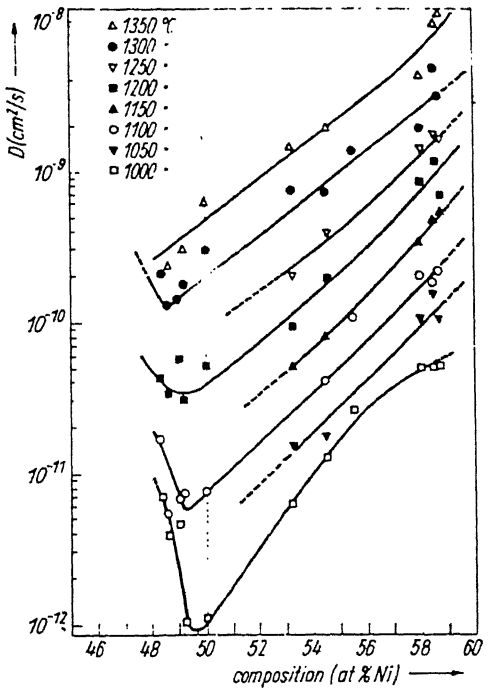

Fig 2.9 :Variation of self diffusion coefficient with composition in NiAl

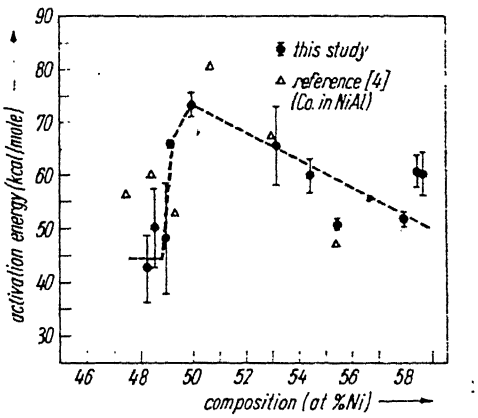

Fig 2.10 : Variation of activation energy with composition in NiAl.

least two or three lattice sites are involved in the formation of thermal defects due to which free energy of non-stoichiometric compound is lower than stoichiometric compounds. It is the consequence of these analysis that as temperature is increased, composition further removed from stoichiometric become more stable. This shows the variation in composition at which the minimum in D occur.

Wasilewski et al. (32) further showed that the resistivity of NiAl alloys shows a minimum at 50.4 at%Al. This is similar to the suggestion given by Cooper (4)

2.7 Mechanical Properties of Intermetallic Compound NiAl

Intermetallic compound NiAl having a good corrosion properties, high hardness, high melting point and some degree of covalency. Mechanical properties of NiAl depends upon several factors:

(i) Composition of NiAl compound.

(ii) Grain size of NiAl compound.

(iii) Whether NiAl is polycrystal or single crystal and orientation of single crystal also affect on the mechanical properties.

(iv) Temperature of deformation.

There may be some other factors which will affect the mechanical properties of NiAl. According to Grala (33) room temperature strength of NiAl decreases with increase in aluminium content except for the 30 w/o Al alloy for which value of strength is equal to 28.14 Kg/mm^2 while for other alloys strength decreases from an average of 19.73 kg/mm^2 for 25 w/o Al to 11.95 kg/mm for the 28 w/o Al to 9.98 kg/mm^2 for the 31.5 w/o Al alloy. Variation of tensile strength versus composition is given in Figure (2.11). According to Pascoe et al (34) polycrystals of different composition and single crystal (stoichiometric composition exhibited the three stages temperature dependence of the yield stress typical of b.c.c. alloys. The main effect of non-stoichiometry was increase the thermal contribution to the yield stress. The strengthening produced by vacancies (Al-rich alloys) was greater than that produced by substitutional atoms.

In general for most of alloys stress/strain obey the empirical equation (35)

$$\sigma = K \varepsilon^n \qquad (2.1)$$

K,n constants that depends on the material test temperature and strain rate.

Lantenshlager (36) reported that deviation from stoichiometry increased strength, however such behaviour

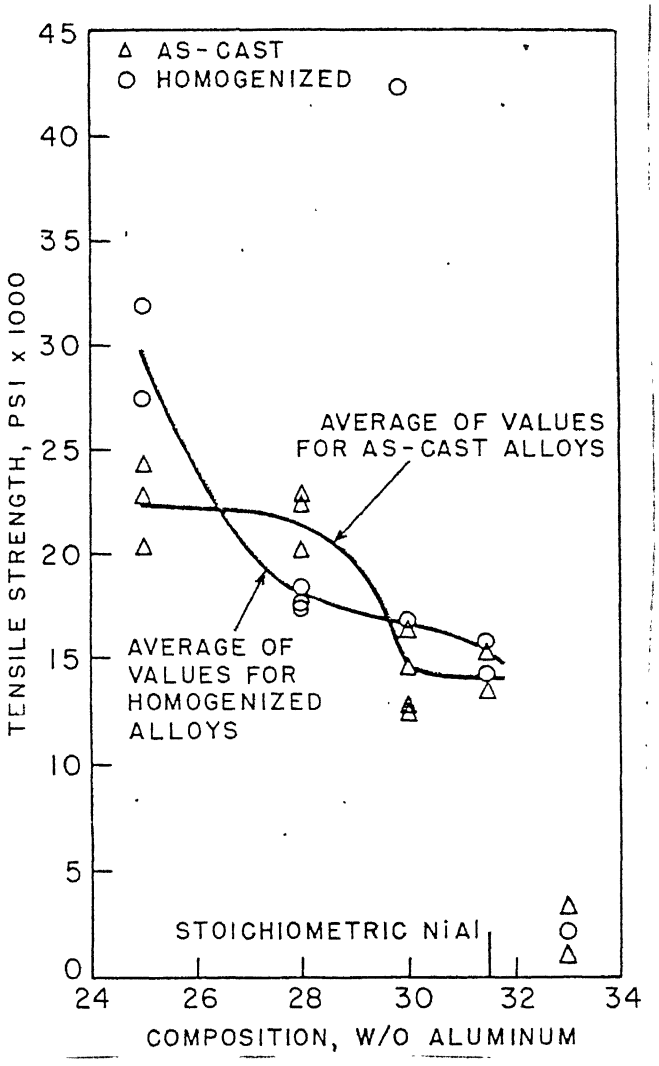

1 Psi= .067 Kg/cm^2

Fig 2.11: Variation of tensile strength with compsition in NiAl

was not continuous as strength peaked at ~52 at% Al and ~42 at%Al with the Hypostochiometric material being the strongest. Ball and Smallman (37) showed for a narrow composition range (47.9 to 51.1 Alat%) that initial flow stress of polycrystalline near stoichiometric is greatest for temperatures exceeding 900K. While Pascoe and Newey (38) found that 0.2% proof stress of 48.9 at% Al was considerable less than that of either 43 at%Al or 53at%Al. Yang and Dodd (39) examined six intermetallic compounds from 45 at% Al to 54 at%Al and found that as the temperature increased, three groups of relative strength appeared in which extreme hypostoichiometric compound was strongest, extreme hyperstoichiometric compound is weakest and rest of compositions are approxinately of same strength. Whittenberger (40) reported that strength for hyperstoichiometric NiAl is less than that of either the 49.3 at%Al or 43.9 at%Al NiAl.

Flow stress-strain rate data for NiAl can be well described by power law creep

$$\dot{\varepsilon} = A\sigma^{n} \qquad (2.2)$$

A is a constant and n stress exponent far creep.

Whittenberger (40) reported that activation energy for creep for most of alloys is same except extreme hypo and hyper stoichiometric alloy where activation energy slightly decreases with increase in Al content and it increases with decrease in Al content. He also reported

that creep strength is independent of composition for Al/Ni $\leq$ 1.03. It is shown in Figure (2.12).

Shankar et al (41) reported that activation energy for interdiffusion varies greatly with concentration. Some estimated flow stresses for different composition at strain rates 1.33×10^{-5} and 1.33×10^{-6} for temperatures 1200K and 1300K are given in Table (2.3) (40).

According to Grala (38) grain coarsening decreases the strength of NiAl. He further reported that strength and ductility of stoichiometric NiAl can be increased by the addition of small amount of Mo. This occurs due to reduction in grain size and precipitation of second phase particle. Strength and ductility of stoichiometric NiAl also increases at 815^{o}C. Whittenberger (40) explained the concept of creep and transitioned from normal clumb/glide mechanism to diffusion creep and the basis of subgrain.

According to Sherby et al (42) the subgrain size can have a profound effect on the steady state creep:

$$\dot{\varepsilon} \propto (\lambda/b)^3 \quad (\sigma/E)^8 \quad D_{eff} \qquad (2.3)$$

where b is the magnitude of burger vector, E is dynamic elastic modulus and D_{eff} is an effective diffusion coefficient.

The existence of subgrains in NiAl and from equation (2.3) it can be concluded that creep in NiAl intermetallic compound is controlled by subgrain size. Whittenberger (40)

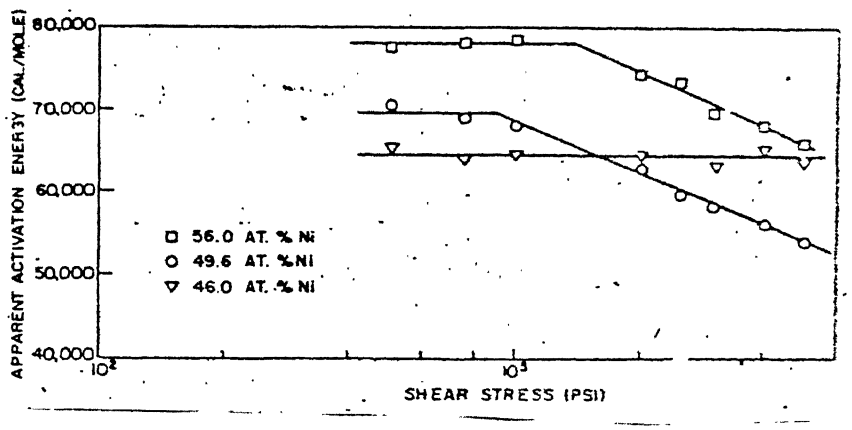

Fig 2.12:Apparent activation energy vs flow stress plot

Table 2.3 : Estimated Flow Stresses necessary to Produce Strain Rate of 1.33×10^{-5} and $1.33 \times 10^{-6} sec^{-1}$ in NiAl

Composition		Flow Stress at (MPa)			
Al	Al/Ni	1200K		1300K	
		1.33×10^{-5} sec^{-1}*	1.33×10^{-6} sec^{-1}	1.33×10^{-5} sec^{-1}	1.33×10^{-6} sec^{-1}
54	1.17	40	20	21	10
54	1.17	24	--	13	--
52.7	1.12	42	26	24.5	14
52	1.08	46	27	35	18
50.4	1.02	31	--	17.5	--
50.25	1.01	61.5	28.5	35.5	16
50.00	1.00	52	33	33	20
49.91	1.00	--	--	30	20.5
49.2	0.97	45	31	31	22
45	0.82	73	40	39	22
44	0.79	38	--	19	--
43.9	0.79	--	--	29	19

* Strain rate.

concluded that

(i) For lower temperature, high strain rate conditions, creep seems to be controlled by the formation of subgrains.

(ii) For higher temperatures and low strain rate creep can be affected by grain size.

Ball (43) reported that grain size had little influence on the proof stress and according to him mode of fracture was generally intercrystalline in very fine polycrystals (grain dia = 50 μm) but and increase in grain size resulted in increased tendency to transcrystalline fracture. They further reported that fracture stress, strain to fracture and strain hardening exponent n decreased with increasing grain size. Effect of grain size on polycrystalline Ni-48.9 at% Al at 295K is given in Table (2.4) (38).

Schulson (44) suggested that tensile ductility may be imparted to brittle polycrystals by refining them to grain size smaller than a initial value. The finer is the grain size below the critical value, greater the tensile ductility. Assuming that the length of microcrack is proportional to grain size, the critical grain size was formulated as

$$d_c = \left(\frac{Y_{KIC} - K_Y}{\sigma_i}\right)^2 \qquad (2.4)$$

where y is a geometrical parameter equal to unity and K_{IC} is the plain strain fracture toughness of the aggregate, K_y and σ_i are Hall Petch parameters.

According to Schulson et al (45) if grains larger than critical value are not completely brittle, it implies that some plasticity is required for crack nucleation. They did tensile testing of NiAl at 673K and found that ductility is very low and essentially independent of grain size for aggregate having grain size larger than 20μ m. While grains of aggregate which are finer than 20μ m ductility increases sharply with decrease in grain size. For all grain sizes, fracture occurs in a brittle manner through a combination of intergranular decohesion and transgranular cleavage. It is shown in Figure (2.13).

Ball and Smallman (37) found that polycrystals of NiAl become ductile at a temperature nearesr above 0.45 T_m. They also reported that initial flow stress decreases with increase in temperature and they found that stoichiometric alloy has lower strength at lower temperature but it is maintained upto a temperature greater than at which alloys of non-stoichiometric composition soften.

Table 2.4 : Effect of Grain Size on the Mechanical Properties of Polycrystalline Ni-48.9 at% Al at 295K

Annealing Condition		Grain Dia m	Micro-Hardness $Kg\ mm^{-2}$	Proof stress $Kgmm^{-2}$	Fracture stress $Kg\ mm^{-2}$	Strain to Fracture	Strain Hardening Exponent
Time, h	Temp, K						
As extruded	--	45	-	34.1	90	16	
1	1173	43	300	27.2	87	17	0.44
1	1373	45	290	27.5	90	18	
1	1473	75	300	27.0	71	13	
1	1573	125	300	25.4	72	12	0.39
1	1673	240	340	28.3	64	10	
1	1773	350	325	31.2	57	7	
24	1773	300	320	24.6	60	9	0.27
24 (Prestrained crystal)	1773	011	320	20.8	57	12	hardening

According to Van Mises (46) five independent slip systems are required for general ductility in a polycrystalline aggregate. Pascoe et al (38) did experiment an polycrystalline material of these basic composition 43.0, 48.9 and 53.0 at%Al and they reported that a material with sufficient slip system can fail in a brittle manner if cracks are created and propagated at stress lower than that required for general deformation.

Ball and Smallman (37) compressed single crystals along two directions < 110 > and < 100> for compositions greater than 50at% Ni and they observed that in < 110 > direction extreme ductility and at lower temperature it retain its ductility while polycrystalline material behave in a brittle manner. They also reported that compression along 100 direction initial flow stress increases and also sinking behaviour. According to Van Mises (46) brittle behaviour of polycrystalline material occur due to grain boundaries because of the incompatibility of shape change in neighbouring grains which results from an inadequate number of independent deformation modes at temperature below 0.45 T_m for the general plasticity of polycrystalline aggregates. Brittle behaviour of single crystal in < 100 > direction is consistent with the operation of < 100> burger vector which would lead to and in sufficiency of slip modes and a tendency to brittle behaviour.

Ball and Smallman (37) concluded that polycrystalline NiAl is hard and extremely brittle at temperatures below 0.45 T_m but becomes soft and ductile above this temperature. According to Grala (33) NiAl behaves in a ductile manner at high temperatures in contrast to extremely brittle behaviour of these alloys at room temperature. He found that for stoichiometric alloy strength is maximum at 650^{o}C. Vander Voort et al. (47) determined the flow stress at five strain rate for NiAl alloys as a function of temperature and they reported that deformation is thermally activated and initial flow stress far NiAl alloys decreases as temperature increases. Figure (2.14) shows the plot of shear stress vs. temperature for 49.6 wt% Ni alloy.

Vander Voot et al. (47) predicted that for stoichiometric NiAl and Ni-rich NiAl alloy at least two deformation mechanism occur. One at high temperature and other at lower temperature. At high temperature two most likely deformation mechanism are there. Either the climb of dislocation or viscous flow mechanism. They found that most probable mechanism is viscous flow mechanism. According to Vander Voot et al (47) mechanism of deformation below 1200^{o}C for stoichiometric NiAl alloy and Ni-rich NiAl is different than the mechanism at high temperature which is diffusion controlled viscous creep mechanism while in Al-rich NiAl alloy viscous creep mechanism continued to exhibit over the entire range.

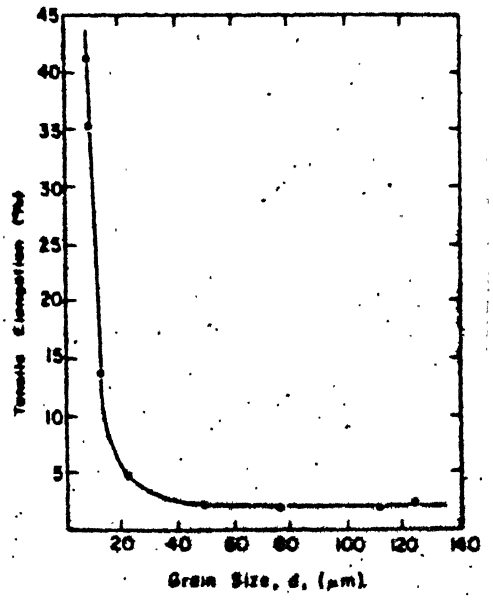

1 Psi= .067 Kg/cm^2

Fig 2.13: Elongation vs grain size of NiAl

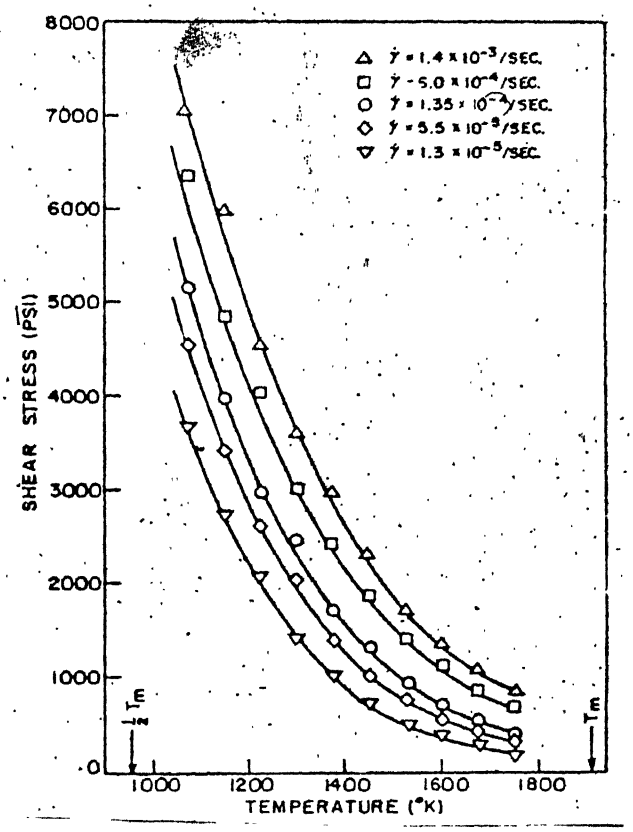

1 Psi=.067 Kg/cm^2

Fig 2.14;Flow stress vs temperature for 49.6 at % Ni alloy

2.8 Improvement in Ductility and Toughness of NiAl

2.8.1 Alloying Additions

Alloying additions greater than about 1at% may be used in several ways: to change the crystal structure to one of higher symmetry and/or smaller unit cell size, to promote the operation of different or additional slip systems, to produce a second phase, or to make the alloy susceptible to a (stress induced) phase transformation.

For cubic crystals such as NiAl which are brittle because they lack sufficient slip systems, macroalloying may be used to promote the operation of a different slip vector. According to Baker and Munroe (48), it is possible that macroalloying of NiAl with iron will produce < 111 > slip and thus, some ductility. Inone et al. (49) reported that melt spun ribbons of 82 structured Ni-30 Al-20Fe of 4 μm grain size exhibited 5% plastic strain at room temperature. They attributed this ductility to a combination of grain size refinement and suppression of both ordering and ground boundary segregation.Law and Blackburn (50) have also examined the effects of adding ternary addition to near-stoichiometric NiAl. They found that with the additions of ~ 5 at% chromium or manganese the slip vector changed from <001> to <111> . They noted that, although <111> slip satisfies the general requirement for plasticity, no significant measure in ductility was observed (although a change from intergranular fracture to transgranular cleavage w noted) and this was attributed to the dislocation mechanisms involved in deformation process, especially the generation and

mobility of dislocations.

2.8.2 Microstructural Control

Polycrystals of NiAl are brittle, albeit for different reasons, single crystal are ductile.

Ductility can also be enhanced or promoted by grain size refinement. Schulson (44) suggested applying to NiAl the concept that a critical grain size exists below which the stress to nucleate cracks (which are of the order of the grain size) is less than the stress to propagate them (45). And indeed, it was found that at 400^{o}C grain sizes below 20μm showed increase ductility (upto 40% elongation) (51). An interesting feature of the brittle to ductile transition in this alloy is the extent of ductility. It is possible that while stable microcracks allowed the initial elongation (to say, 5%), the subsequent extensive ductility could have been the results of the activation of additional slip vectors $<111>$ at higher stress levels. Of course, the additional slip systems may only have operated in small volumes of material near grain boundaries.

Fine grain sizes also lead to slip homogenization and greater ductility. Thus grain refinement should in theory, work for any intermetallic. The problem is that the grain size required to produce ductility may be very small (possibly sub micron) and difficult to achieve.

Although Boron is known to improve drastically ductility to Ni_3Al but it has not been examined for NiAl.

2.9 Scope of Present Investigation

Literature review reveals that a little study has been done on the phase stability of intermetallic compound NiAl with solute additions. The review of literature also shows that solubility of NiAl with Ta has not been established. Effect of boron on the phase stability and mechanical properties of β -phase has not been stated. The present investigation included phase diagram studies of boron doped and boron free alloys, at two equilibriation temperatures, 1200^{o}C and 1000^{o}C. Compression testing was also proposed for alloys to study the effect of Ta and Boron on the mechanical properties of intermetallic compound NiAl. A comparison was made between alloys not containing boron and containing boron.

CHAPTER 3

EXPERIMENTAL TECHNIQUES

3.1 Alloy Preparation

3.1.1 Alloys Without Boron

The starting materials for this category alloys were elemental Ni of 99.99% purity, aluminium of 99.99% purity and tantalum of 99.9% purity. Composition of alloys not containing boron are given in Table (3.1).

3.1.2 Alloys Containing Boron

The starting material was boron doped Ni_3Al which was supplied by Defence Metallurgy Research Laboratory, Hyderabad. Boron content in Ni_3Al was known to be 500 ppm. To prepare the alloy, aluminium and tantalum were added in Ni_3Al as per the requirement. In weight percentage calculation boron was neglected because of its little weight. Composition of alloys containing boron are given in Table (3.2).

3.2 Melting

The alloys were melted in argon atmosphere in a water cooled copper crucible using tungsten rod as non-consumable electrode in an arc melting furnace. The

Table 3.1 : Compositions of Alloys not containing Boron

Alloys composition in Atomic Percentage		Ni wt%	Al wt%	Ta wt%
Ni at%	Ta at%			
50	0	68.51	31.49	0
50	5	58.07	24.02	17.91
50	1	66.14	29.78	4.08
50	0.06	69.08	30.45	2.481
63.5	1.5	75.41	19.10	5.49

Table 3.2 : Compositions of Alloys containing Boron:

Alloys composition in atomic percentage		Ni	Al	Ta
Nickel atom%	Ta at%	wt%	wt%	wt%
50	5	58.07	24.02	17.91
50	1	66.14	29.78	4.08
50	.06	69.08	30.45	2.481

ingot weighing 20 gms was turned over and remelted. This operation was carried out three times. The alloys were weighed once again to observe weight loss. Next they were cut by a diamond into atleast three parts in Table (3.3) lists the melting loss of alloys.

3.3 Homogenization of Alloys

The alloys were vacuum sealed in fused silica tube under vacuum of 10^{-2} torr or 10^{-3} torr. Each sealed tube was put in the furnace at a temperature of 1200°C for 9.5 days. Temperature of the furnace was maintained within ±2°C. After completing the homogenization samples were water quenched.

Homogenization time was determined by experimenting on a boron doped 5at% Ta alloys. Initially it was water quenched from 1100°C after 9 days. After that it was kept at 1200°C and after every 3 consecutive days of homogenization, it was water quenched. Lattice parameter measurement was done. It was found out that homogenization was effected after 9 days. So all the samples were homogenized for 9.5 days at 1200°C. Lattice parameter vs. homogenisation time plot for 50 at%Ni, 5.0at%Ta with B is given in Fig.(3.1).

3.4 Equilibriation at 1000°C

One of the 3 pieces of each sample homogenized and equilibriated at 1200°C was taken out for annealing

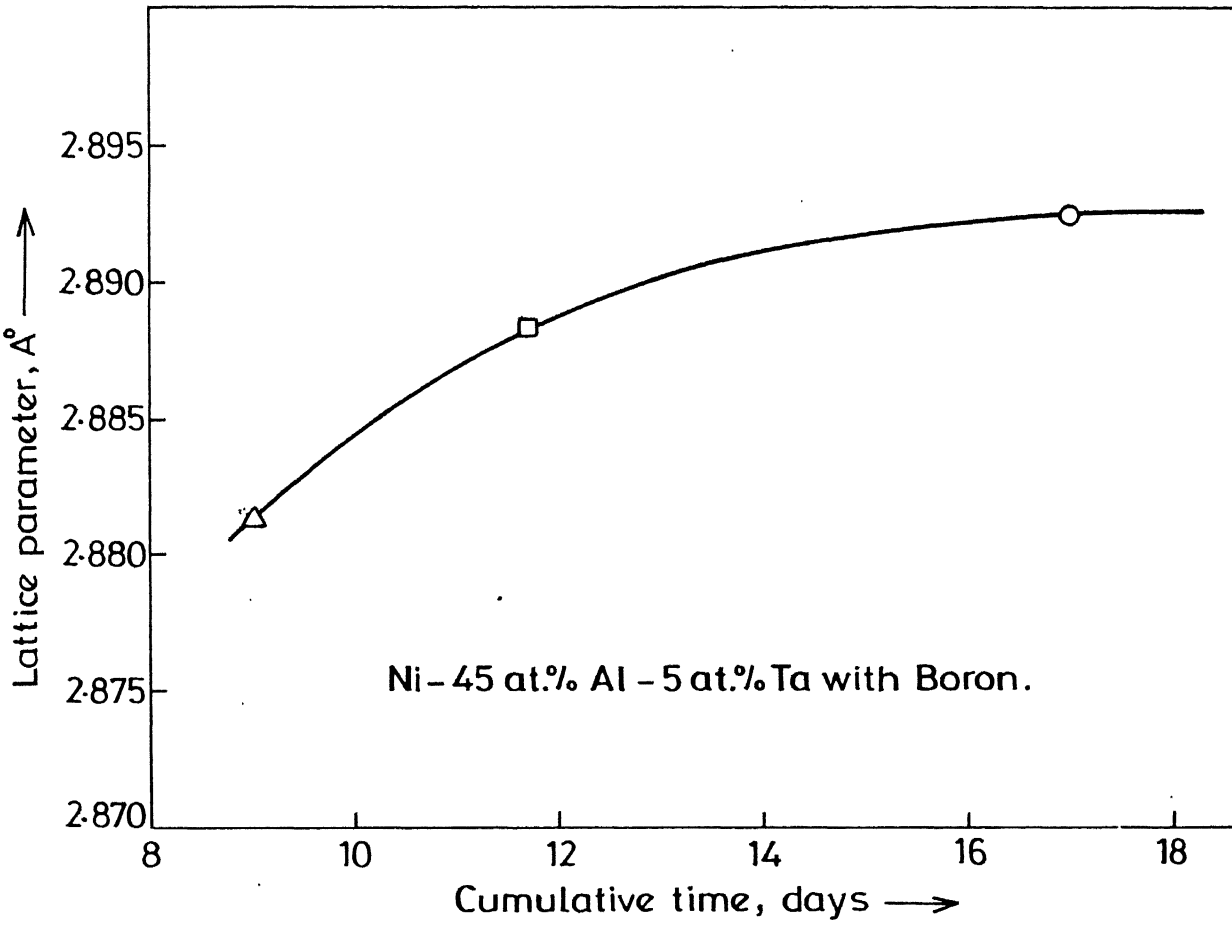

Fig. 3·1 Variation of lattice parameter with homogenisation time.

△ Cast ingot Homogenised 1100°C for 9 days.

□ Sample Homogenised at 1100°C further homogenised at 1200°C for 3-6 days.

○ Sample Homogenised at 1100°C further homogenised at 1200°C for 9 days.

Table 3.3 : Melting Loss in Alloys

Alloy composition at% Ni	at% Ta	Containing Boron	Wt.before melting	Wt.after melting	% Melting Loss
50	0.6	No	20.0023	19.9768	0.1
50	1.0	No	19.9965	19.7442	1.2
50	5.0	No	19.9288	19.7876	0.7
50	0.6	Yes	19.8288	19.6876	0.7
50	1.0	Yes	19.9932	19.8053	0.9
63.5	1.5	No	19.79.13	19.7657	0.1
50	5.0	Yes	19.9998	19.8114	0.9
50	0.0	No	14.9876	14.8732	0.7

*Ref. (52).

at 1000°C. The piece was vacuum sealed in quartz tube and kept at 1000°C for 10 days. The furnace was maintained at 1000°C with an accuracy of ±2.0°C.

3.5 X-ray Diffraction

3.5.1 Powder Sample Preparation

Powder sample for X-ray diffraction was prepared by hammering the small piece of button which was cut by diamond saw. These powder sample was sealed under vacuum in quartz tube and then heated to temperature of equilibrium for 15 to 20 minutes in order to relieve the strains in the material and then water quenched.

3.5.2 X-ray Diffraction Conditions

The X-ray diffraction work was carried out on a Rieh Seifert Isodebye flux 2002 diffractometer. A graphite crystal monochromator was used to receive monochromatic radiations.

3.5.2.1 Selection of Target Material

It is well known that if one uses a target material with smaller characteristic radiation wavelength ($K\alpha$), the peaks will be shifted to lower angles. Hence, there will be more number of peaks in the diffractograph. The more the number of peaks the more the number of points in Nelson Reley plot. Out of two target materials, Cu and Cr available in X-ray Lab, was preferred.

3.5.2.2 Range of '2θ' used for Scanning

Initially the diffraction patterns of all samples were taken over the entire range of 2θ (20° - 150°) using Cu target. In the second step slow scanning was near the peaks in order to get more accurate 2θ. Values for the peak positions.

3.5.2.3 Diffractometer Conditions

The diffractometer conditions are listed below:

Rapid scanning:

Voltage = 30 KV

Current = 20 mA

Scanning speed = 3°/min (in 2θ value)

Chart speed = 30 mm/min

Time constant = 3 sec.

Counts per second = 200

Beam slit = 2 mm

Receiving slit = 0.3 mm.

However, parameters such as scanning speed, chart speed and counts per second were different for peak to peak scanning.

Scanning speed = 0.6°/min

Counts speed = 15 min/min

Counts per second = Changed with intensity of peaks.

To find out the error in the machine a standard silicon sample was scanned at 0.6°/min. Error was calculated by

subtracting recorded peak values from calculated peak values.

3.6 Optical Microscopy

Alloys were hot mounted and metallographically polished and etched. The etching reagent was used. Alcoholic Ferric Chloride (anhydrous $FeCl_3$ 5 gm, HCl 10 ml, Ethanol 100 ml). Etching time was approximately 15 to 20 seconds at room temperature.

3.7 Microhardness Measurements

The microhardness values of β-phase were determined by Leitz microhardness tester. A load of 25 gram and a diamond indentor was employed for indentation of the samples. Several indentations were made on the specimens and average of microhardness values was taken.

3.8 Compression Tests

Compression testing specimens typically 3.8x3.8x4.2 mm were cut by diamond saw. Belt polisher was used to make the surfaces flat. Specimens were deformed at 550^{o}C temperature by means of compression jigs attached to 10 ton MTS unit. Samples were heated with the help of a furnace which surrounded the compression jaws. Temperature was measured with the help of three chromel-alumel thermocouples. Temperature of the furnace was maintained within $\pm$2^{o}C. While samples were not

kept in neutral atmosphere, it did not get oxidise during testing. Testing took around one hour in heating and $1\frac{1}{2}$ hrs in complete loading of the samples. The arrangements of compression testing machine are shown in figure (3.2).

The most reproducible means of measuring the yield strength was found to be a 0.2% proof stress. Strain rate was $10^{-4}sec^{-1}$ and it was constant for all samples.

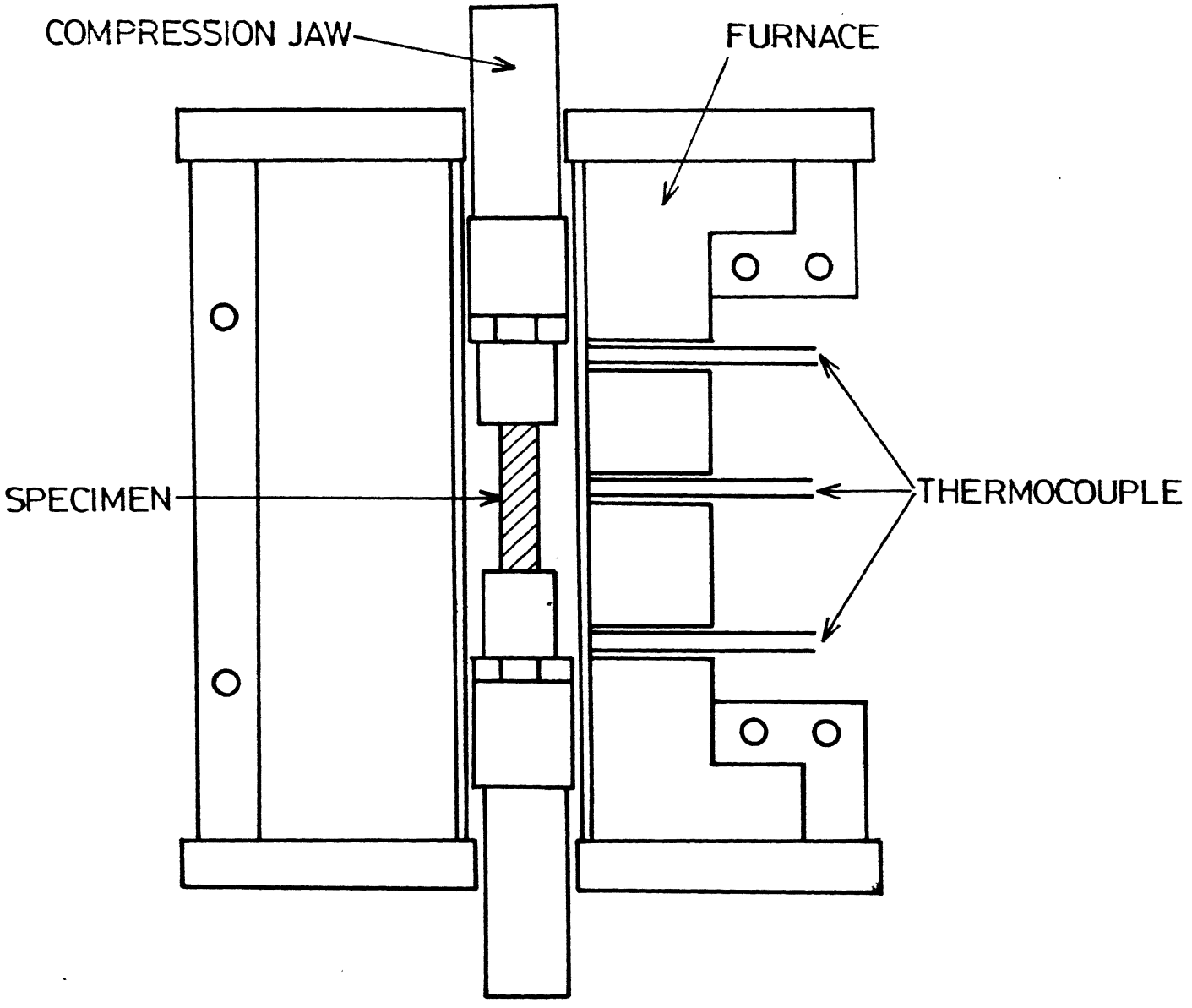

Fig. 3-2 Arrangements of compression testing machine.

CHAPTER 4

RESULTS

4.1 Homogenisation

Homogenisation of alloys was carried out at 1200°C for 9.5 days. Homogenisation time was decided by measuring lattice parameter of alloy containing 5at% Ta, and boron at 1100°C and 1200°C for different days. Plot lattice parameter versus homogenisation time is given in Figure (3.1). It shows that 9.5 days at 1200°C should be adequate for homogenisation.

Micrographs of all alloys equilibriated at 1200°C are shown in Figures (4.1) to (4.6). Tiny black spots in the matrix are either blow holes or inclusions in the samples.

Equiaxed grains of 0.6 at% Ta alloy are of around 75μ. Photomicrograph (Figure 4.1) shows that alloy has a small percentage of precipitating phase on the grain boundaries.

Grain size of alloy (1.0 at% Ta) is approximately 190μ and grains are elongated. Photomicrograph is shown in Figure (4.2).

Photomicrograph of alloy (5 at% Ta) is shown in Figure (4.3). It has grain size around 100μ and grains are elongated. Second phase is also present on the grain boundaries.

Photomicrograph (Figure 4.4) of alloy (0.6 at% Ta, containing boron) shows that there is possibility of a very

amount of second phase while amount of inclusions or blow holes in the sample is very high. Elongated grain size are approximately 83 μ.

Photomicrograph (Figure 4.5) of alloy (1.0 at% Ta, containing boron) reveals that a small amount of precipitating phase is present on the grain boundaries. Size of grains is approximately 31μ and grains are elongated.

Alloy (63.5 at% Ni, 1.5 at% Ta) has two phase structure. Grains are elongated and size is around 170μ . Photomicrograph is shown in Figure (4.6).

4.2 Annealing at 1000°C

Alloys were equilibriated at 1000°C for 10 days. Photomicrographs of all alloys are shown from Figure (4.7) to Figure (4.12). Small black spots are blow holes or inclusions in the sample.

In the 0.6 Ta alloy the grain size is approximately 200μ . A phase is precipitating out on the grain boundaries. Grains are equiaxed. The photomicrograph is shown in Figure (4.7).

A precipitating phase is present on these grain boundaries. Second phase is very less in amount. Grains are elongated in shape and grain size is approximately 200 μ. Photomicrograph is shown in Figure (4.8).

Photomicrograph (Figure 4.9) of alloy 5 at% Ta reveals that amount of second phase is very high and it is present as white patches in the matrix. There is one more phase which has tree type shape.

Photomicrograph (Figure 4.10) of alloy 0.6 at% Ta with boron reveals that a precipitating phase is present on the grain boundaries. Black spots with tail can be seen in the grains, which may be created by chipping out of inclusions during polishing. Grains elongated in shape, are approximately 275μ in size.

Photomicrograph (Fig.4.11) of alloy 1.0at%Ta with boron shows that amount of second phase is very small. Grains elongated in shape, are approximately 150μ in size. Black spots with tail can be seen in the grain as well as on the grains, which may be created by chipping out of inclusions during polishing.

Photomicrograph (Figure 4.12) of alloy 63.5 at% Ni, 1.5 at% Ta shows that it has three phase structure. One phase is elliptical in shape and other has plate type of shape.

4.3 Lattice Parameter Measurement

To measure the precise lattice parameter a correction factor is to be calculated to take care the error in goniometer. To determine the correction factor, X-ray diffraction of Si standard was taken. The peak positions were subtracted from calculated peak positions. Errors near to

Fig 4.2:Photomicrograph of 50 at %Ni, 0.6 at % Ta alloy at 1200 °C,200X

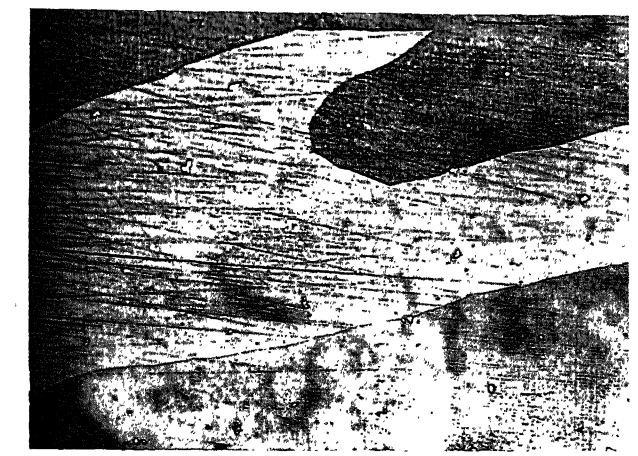

Fig 4.1:Photomicrograph of 50 at% Ni,1.0at% Ta alloy at 1200 °C,200X

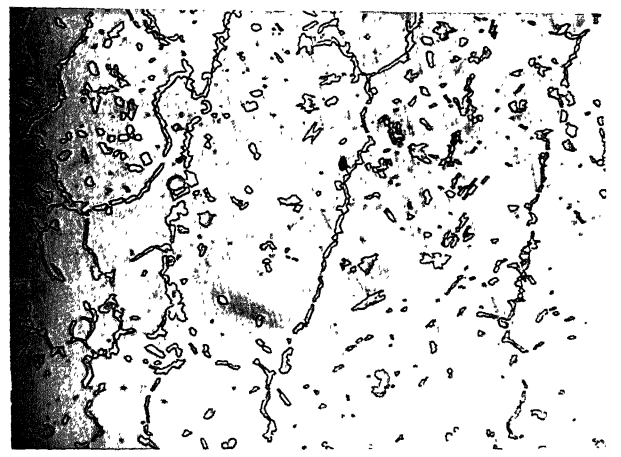

Fig 4.3; Photomicrograph of 50 at% Ni,5.0 at% Ta alloy at 1200 °C, 200X

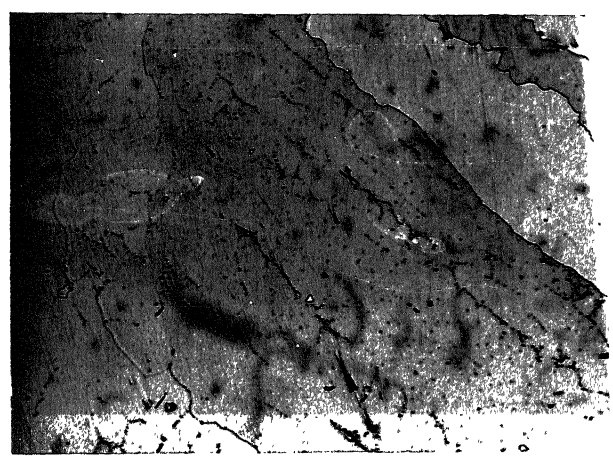

Fig 4.4: Photomicrograph of 50 at% Ni, 0.6 at5 Ta with B alloy at 1200 °C,200X

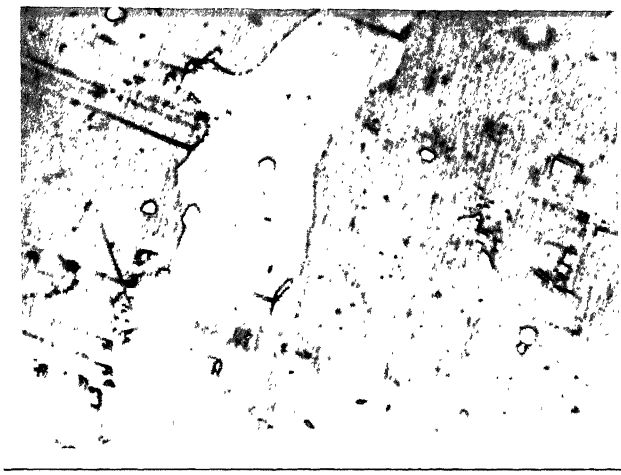

Fig 4.5 : Photomicrograph of 50 at% Ni,1.0 at% Ta with B alloy at 1200 C,500x

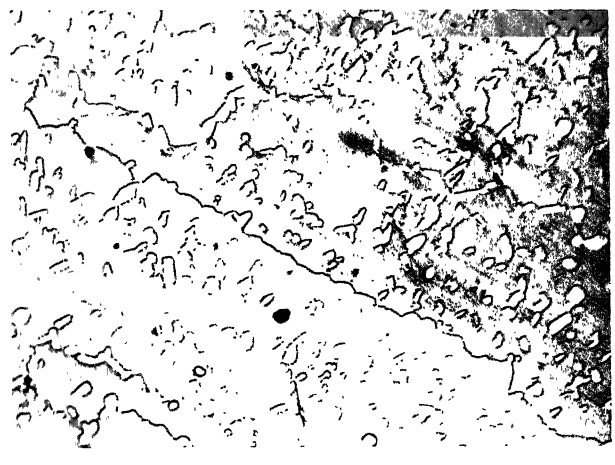

Fig 4.6 : Photomicrograph of 63.5 at% Ni, 1.5at% Ta alloy at 1200 C, 100x

Fig 4.7 : Photomicrograph of 50 at% Ni, 0.6 at% Ta alloy at 1000 °C, 100X

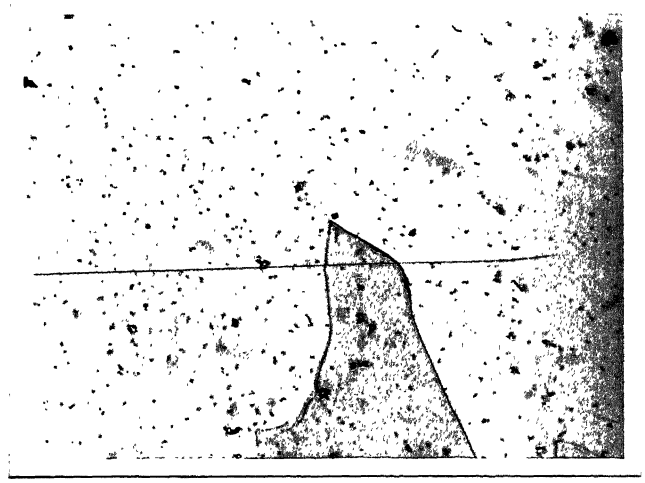

Fig 4.8: Photomicrograph of 50 at% Ni, 1.0 at% Ta alloy at 1000 °C 100X

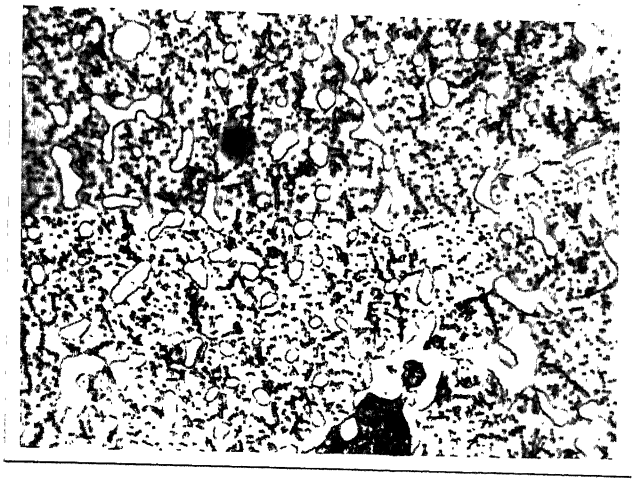

Fig 4.9: Photomicrograph of 50 at% Ni, 5.0 at% Ta alloy at 1000 ℃ 200X

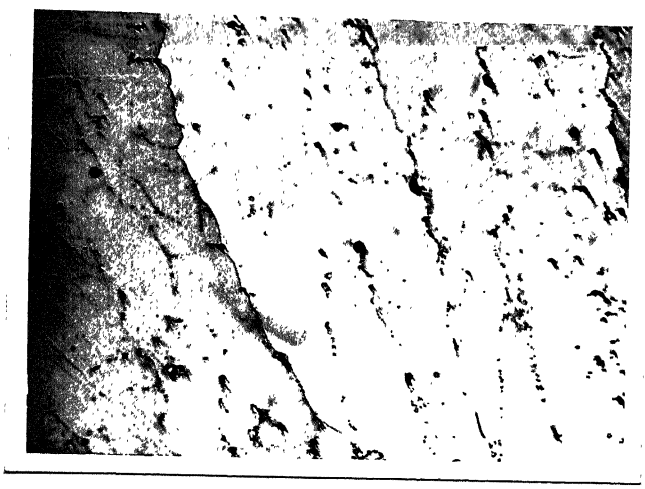

Fig 4.10 ; Photomicrograph of 50 at% Ni,0.6 at5 Ta with B alloy at 1000 °C,200X

Fig 4.11: Photomicrograph of 50 at% Ni, 1.0 at% Ta with B alloy at 1000 °C, 200X

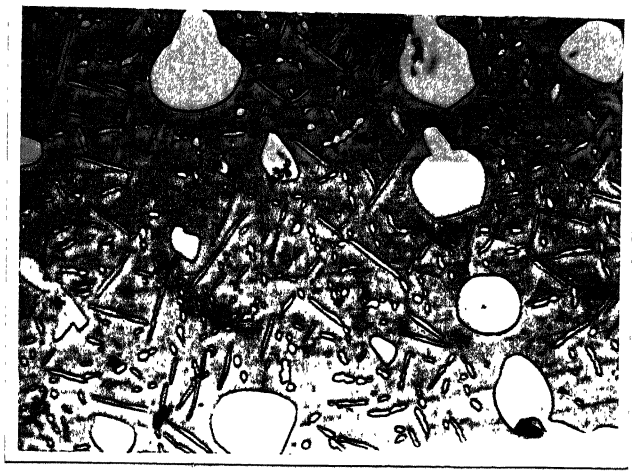

Fig 4.12 : Photomicrograph of 63.5 at% Ni, 1.5 at % Ta alloy at 1000 °C, 500X

peak positions of alloy system, are directly added to 2θ values. Final 2θ values is used for the calculation of lattice parameter.

Lattice parameter is calculated by the formula given below:

$$a = \frac{\lambda}{2\ \mathrm{Sin}\theta}\ x\sqrt{h^2+k^2+l^2}$$

In order to obtain accurate value of the lattice parameter, a value plotted against Nelson-Riley function and extra-plotted to zero.

The Nelson-Riley function is $\mathrm{Cos}^2\theta\ [1/\mathrm{Sin}\theta + 1/\theta]$. Least square computer fit was used to calculate the lattice parameter and to calculate the slope of lattice parameter vs. Nelson-Riley function plot.

4.3.1 Detailed Calculations of Lattice Parameter Measurement

X-ray diffraction tracing of 50at% Ni, 1.0 at% Ta with boron alloy homogenised at 1000°C for 10 days, its powder stress relieved 20/ minutes at 1000°C and of Si standard under of exactly same condition are given in Figure (4.13). Correction factor and lattice parameters are given in Table (4.1) and Table (4.2) respectively. Plot of lattice parameters versus Nelson-Riley function of 50at% Ni, 1.0 at% Ta containing boron is given in Figure (4.14).

Table 4.1 : Calculation of Correction Factor

Observed Value (2θ) of Si			Calculated Value (2θ) of Si			Correction Factor		
CuK	CuK_1	CuK_2	CuK	CuK_1	CuK_2	CuK	CuK_1	CuK_2
28.385			28.4793			0.0943		
47.235			47.3673			0.1323		
56.085			56.2009			0.1159		
69.135			69.2305			0.0953		
	76.2581			76.4166	76.3549		.1585	
	87.93	88.15		88.0798	88.3549		.1498	.2049
	94.83	95.13		95.0085	95.3191		.1785	.1691
	106.5602	116.88		106.7775	107.1609		.2173	.2809
	113.960	114.40		114.1714	114.6117		.2114	.2117
	136.765	137.50		137.0234	137.750		.2584	.2500

Table 4.2 : Calculation of Lattice Parameters of 50 at% Ni, 1.0at% Ta containing Boron

Experimental value (2θ)	Correct value (2θ)	Plane	NRF	q (A^{o})
30.855	30.9493	100	6.912	2.8869
44.250	44.3823	110	4.488	2.8892
55.000	55.1149	111	3.334	2.8867
64.360	64.4553	200	2.602	2.8949
73.175	73.3335	210	2.082	2.8863
81.470	81.6499	211	1.680	2.8865
97.870	98.0485	220	1.074	2.8871
106.150	106.3675	221	0.834	2.8864
114.920	115.1314	310	0.628	2.8873
115.285	115.4967	310	0.620	2.8878
135.040	135.2984	222	0.282	2.8881
135.640	135.8900	222	0.272	2.8873

Precise lattice parameters of the alloy is 2.8874 A^{o} and slope of lattice parameters versus Nelson-Riley function is 7.11×10^{-6}.

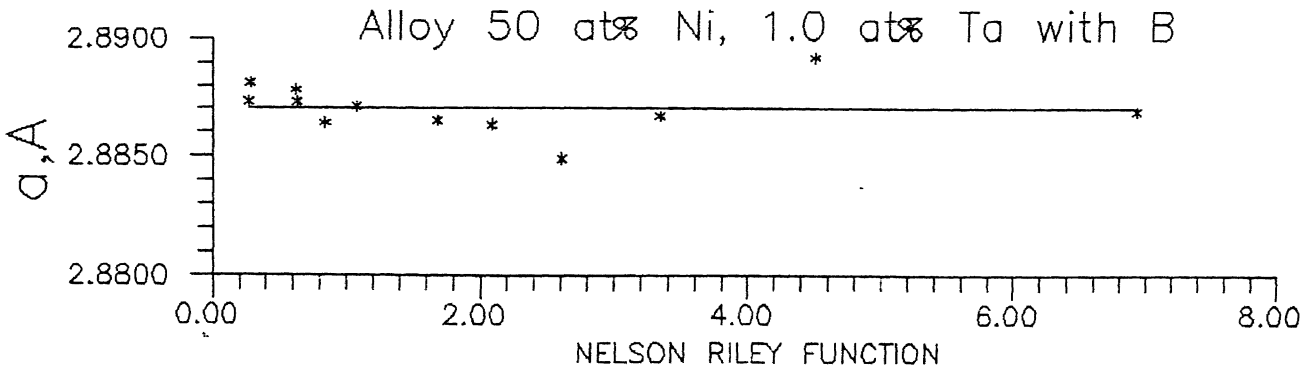

Figure 4.14:Lattice Parameter versus Nelson Riley Function plot

4.3.2 Lattice Parameter of the Alloys at 1200°C

After the alloys were annealed for 9.5 days at 1200°C, lattice parameter measurement was done. Table (4.3) and Table (4.4) list the lattice parameters of alloys with boron and without boron respectively. Plots of lattice parameters versus Nelson-Riley functions for boron free and boron doped alloys are shown in Figure (4.15) and Figure (4.16) respectively. The lattice parameter values of NiAl (with Boron) was taken from the literature (52). Lattice parameter value of NiAl (without Boron) was also taken from the literatures (52).

4.3.3 Lattice Parameters of Alloys Annealed at 1000°C

Alloys were equilibriated at 1000°C for 10 days. Table (4.5) gives the lattice parameters for the alloys at 1000°C. Plots of lattice parameter versus Nelson-Riley functions for boron free and boron doped alloys are given in Figure (4.17). Lattice parameter values of NiAl (with and without boron)were also taken from the literature (52).

4.4 Unknown Peaks in Alloys at Annealing Temperature 1200°C and 1000°C

X-ray diffraction peaks of other phases, apart from NiAl were also present in both alloys containing boron and alloys not containing boron. In some of alloys some phases, which were absent at equilibriating temperature 1200°C, were

Table 4.3 : Lattice Parameters of Alloys (without boron) at 1200°C

Alloy Composition		Lattice parameter (A^{o})	Standard deviation
Ni at%	Ta at%		
50	0	2.8870*	1.3×10^{-3}
50	0.6	2.8874	2.0×10^{-3}
50	1.0	2.8852	1.6×10^{-3}
50	5.0	2.8920	1.3×10^{-3}
63.5	1.5	2.8634	2.5×10^{-3}

*Reference (52).

Table 4.4 : Lattice Parameters of Alloys (with boron) at 1200°C

Alloy Composition		Lattice parameter (A°)	Standard deviation
Ni at%	Ta at%		
50	0	2.886*	1.5×10^{-3}
50	0.6	2.8882	2.5×10^{-3}
50	1.0	2.8857	1.3×10^{-3}
50	5.0	2.8824	1.5×10^{-3}

*Ref. (52).

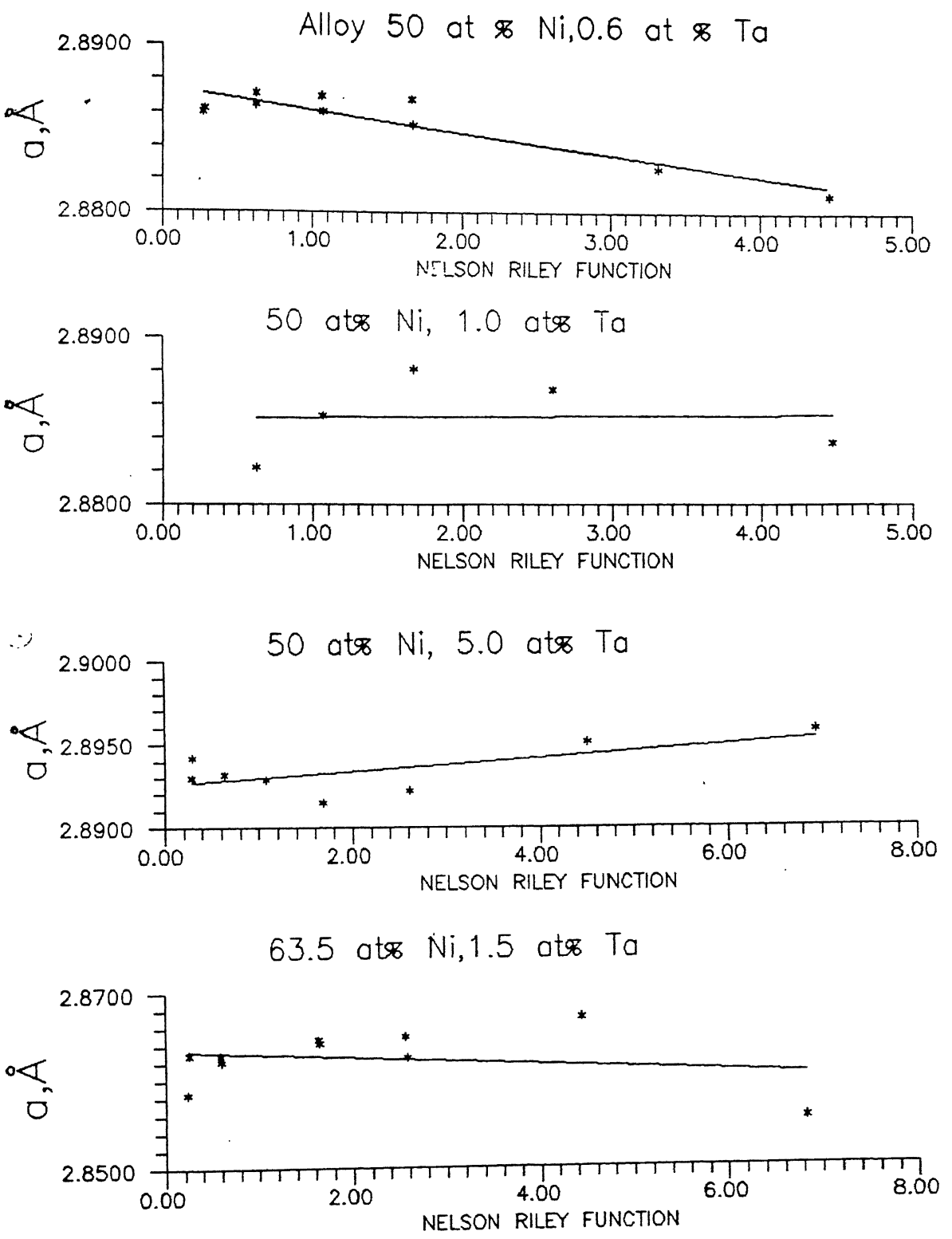

Fig 4.15 : Plots of Lattice Parameter vs Nelson Riley Function for boron free alloys at 1200°C

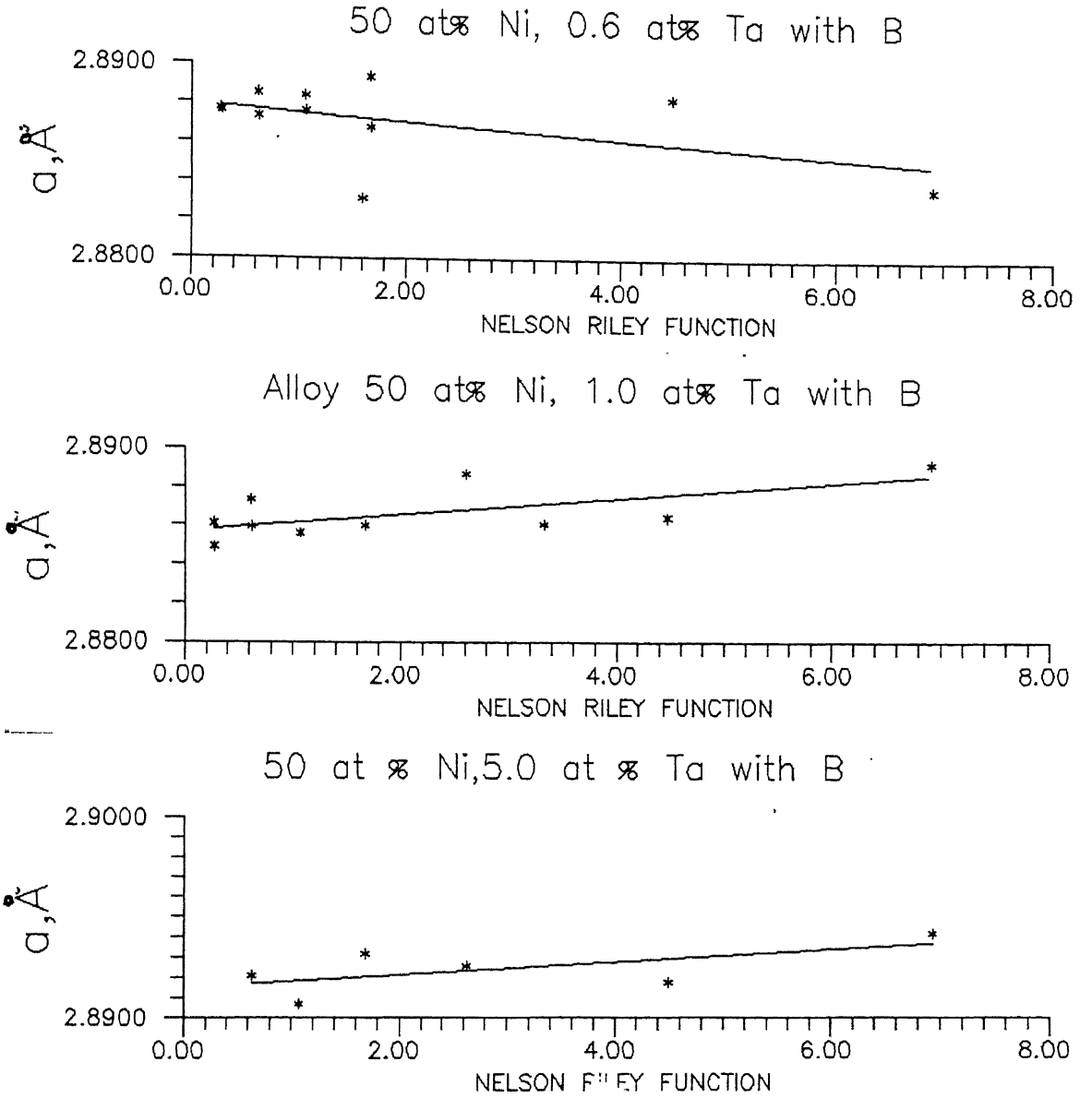

Fig 4.16 : Plots of Lattice Parameter vs Nelson Riley Function for boron doped alloys at 1200°C

Table 4.5 : Lattice Parameters of Alloys at 1000°C

Alloy Composition			Lattice Parameters	Standard Deviation
at%Ni	at%Ta	at% containing boron		
50	0	No	2.8873*	1.5×10^{-3}
50	0.6	No	2.8761	2.9×10^{-3}
50	1.0	No	2.8713	3.5×10^{-3}
50	5.0	No	2.8848	1.00×10^{-3}
50	0	Yes	2.8863*	1.7×10^{-3}
50	0.6	Yes	2.8866	1.30×10^{-3}
50	1.0	Yes	2.8870	1.15×10^{-3}
63.5	1.5	No	2.8648	1.2×10^{-3}

*(Ref. 52).

Alloy 50 at % Ni,0.6 at % Ta

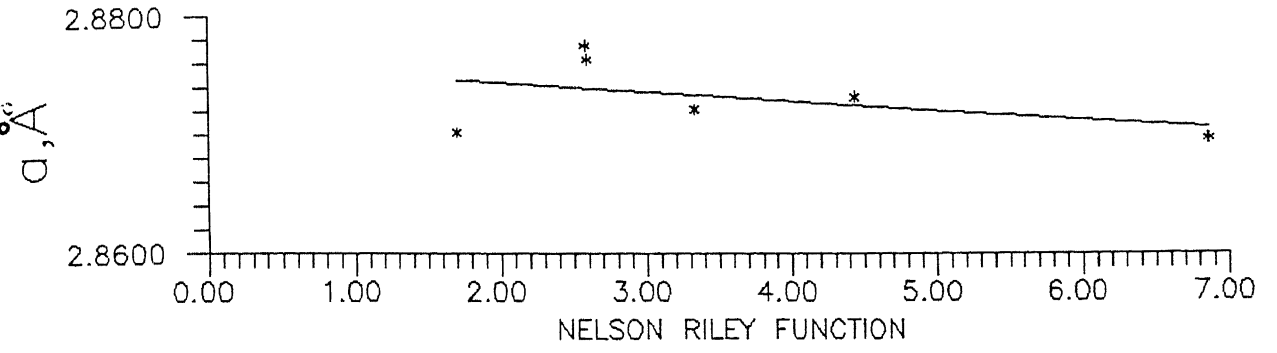

Alloy 50 at % Ni,1.0 at % Ta

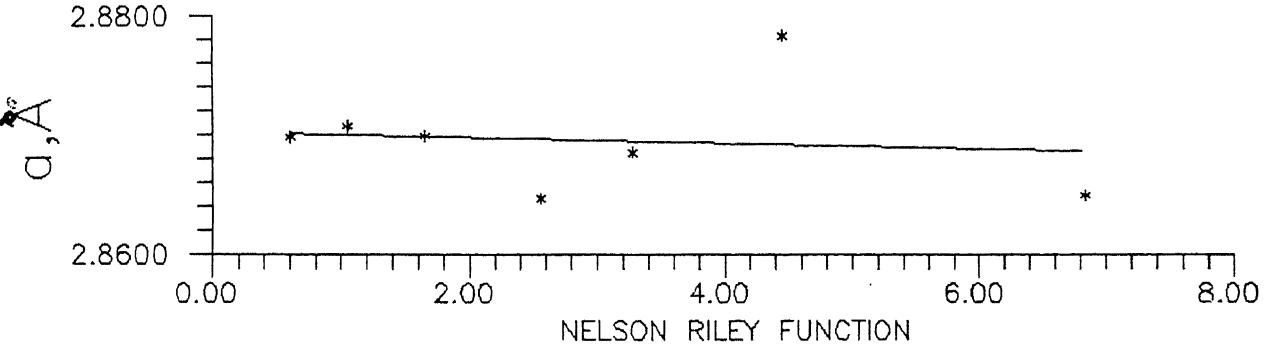

50 at % Ni,5.0 at % Ta

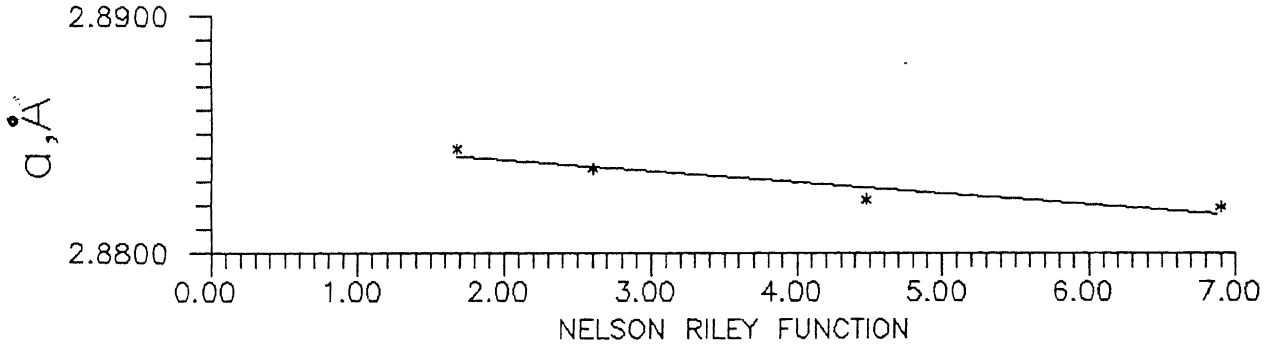

50 at% Ni, 0.6 at% Ta with B

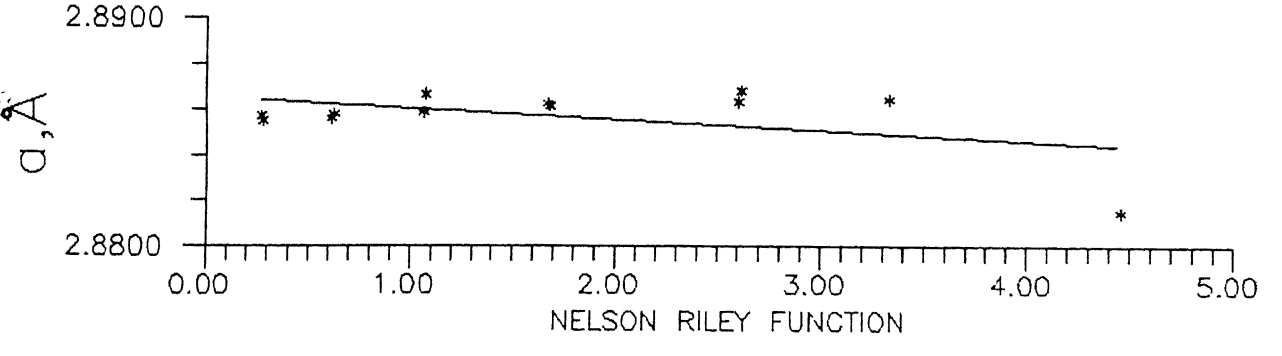

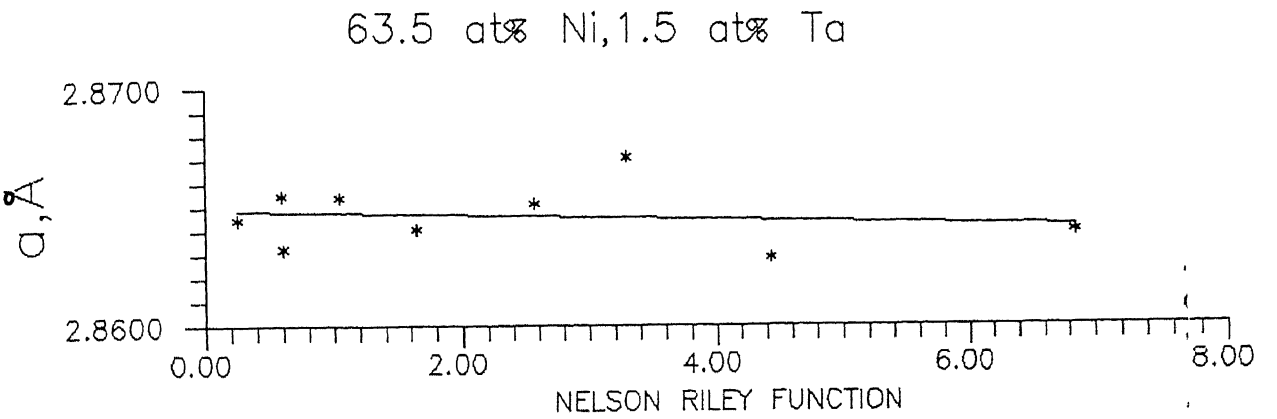

Fig 4.17 : Plots of Lattice Parameter vs Nelson Riley Function for boron free and boron doped alloys at 1000°C

presented at 1000°C. Table (4.6) and Table (4.7) list the unknown peak positions in alloys at 1200°C and 1000°C.

Possible phases in Ni-Al-Ta at the alloy compositions are NiAlTa, Ni_2AlTa, Ni_3Ta, Ni_6AlTa and Ni_3Al. It was found out that apart from the phases mentioned above. Carbides and borides could be possible.

4.5 Microhardness

Microhardness values of matrix phase were measured. Microhardness values of alloys not containing boron and alloys containing boron at 1200°C are listed in Table (4.8) and Table (4.9) respectively.

There was a little decrease in microhardness values of all alloys at 1000°C and they are reported in Table (4.10) and Table (4.11) for alloys without boron and with boron respectively.

4.6 High Temperature Compression Test

Polycrystalline materials of three compositions. Pure NiAl, NiAl containing 1.0 at% Ta and NiAl containing 1.0% at% Ta with boron homogenised at 1200°C for 9.5 days were studied. Flow stress of all samples was measured by during compression testing. Load versus Stroke experimental curves are given in Figure (4.18), Figure (4.19) and Figure (4.20) for alloys. Pure NiAl, 1.0 at% Ta and 1.0at% Ta containing boron respectively. Table (4.12)

and strain rate 10^{-4} sec^{-1}. Photomicrographs of alloys after compression testing are given in Figure (4.21), Figure (4.22) and Figure (4.23). 0.2% proof stress and percentage change in length versus composition plots are given in Figure (4.24) and Figure (4.25) respectively.

4.6 : Unknown Peaks in Alloys at 1200°C

loy Composition														
at%Ta	Containing boron	2θ Value												
0.6	No	35.08	40.675	-										
1.0	No	-	-	-										
5.0	No		39.95	41.342										
1.5	No	-	-	-	43.6723	47.6573	50.7423				72.8585	74.7266	90.7398	96.
0.6	Yes	-	-	-	-	-	-	-	-	-		74.9004	91.0149	96.
1.0	Yes	40.7823						58.9809	70.5303					

Table 4.7 : Extra Phase Diffraction Peaks in Alloys at 1000°C

Alloy Composition at% Ni	at% Ta	Containing boron	2θ Values									
50	0.6	No	34.8993	40.5833				58.6159	70.1625	73.5566 73.8404		
50	1.0	No	35.0045	40.7346			48.7596	58.9309	70.4269	74.0019	88.042	101
50	5.0	No	38.6708	40.2296	41.6646							
3.5	1.5	No	34.9093	40.6523	43.7673			58.6759 58.8959	70.35	73.9816	74.7766	96. 90.
50	0.6	Yes		39.6393	43.4273	45.3273	48.7173		67.868		84.2724	
50	1.0	Yes	-	-	-	-	-	-	-	-	-	-

Table 4.8 : Microhardness Values of Alloys not containing Boron at 1200°C

Alloy Composition		Microhardness (kg/mm^2)
Ni at%	Ta at%	
50	6.0	533*
50	0.6	548
50	1.0	585
50	5.0	689
63.5	1.5	612

*Ref. (52)

Table 4.9 : Microhardness Values of Alloys containing Boron at 1200°C

Alloy Composition		Microhardness (kg/mm^2)
Ni at%	Ta at%	
50	0.6	560
50	1.0	612

Table 4.10 : Microhardness Values of Alloys without Boron at 1000°C

Alloy Composition		Microhardness (kg/mm^2)
Ni at%	Ta at%	
50	0.6	503
50	1.0	514
50	5.0	530
63.5	1.5	548

Table 4.11 : Microhardness Values of Alloys with Boron at 1000°C

Alloy Composition		Microhardness (kg/mm^2)
Ni at%	Ta at%	
50	0.6	507
50	1.0	536

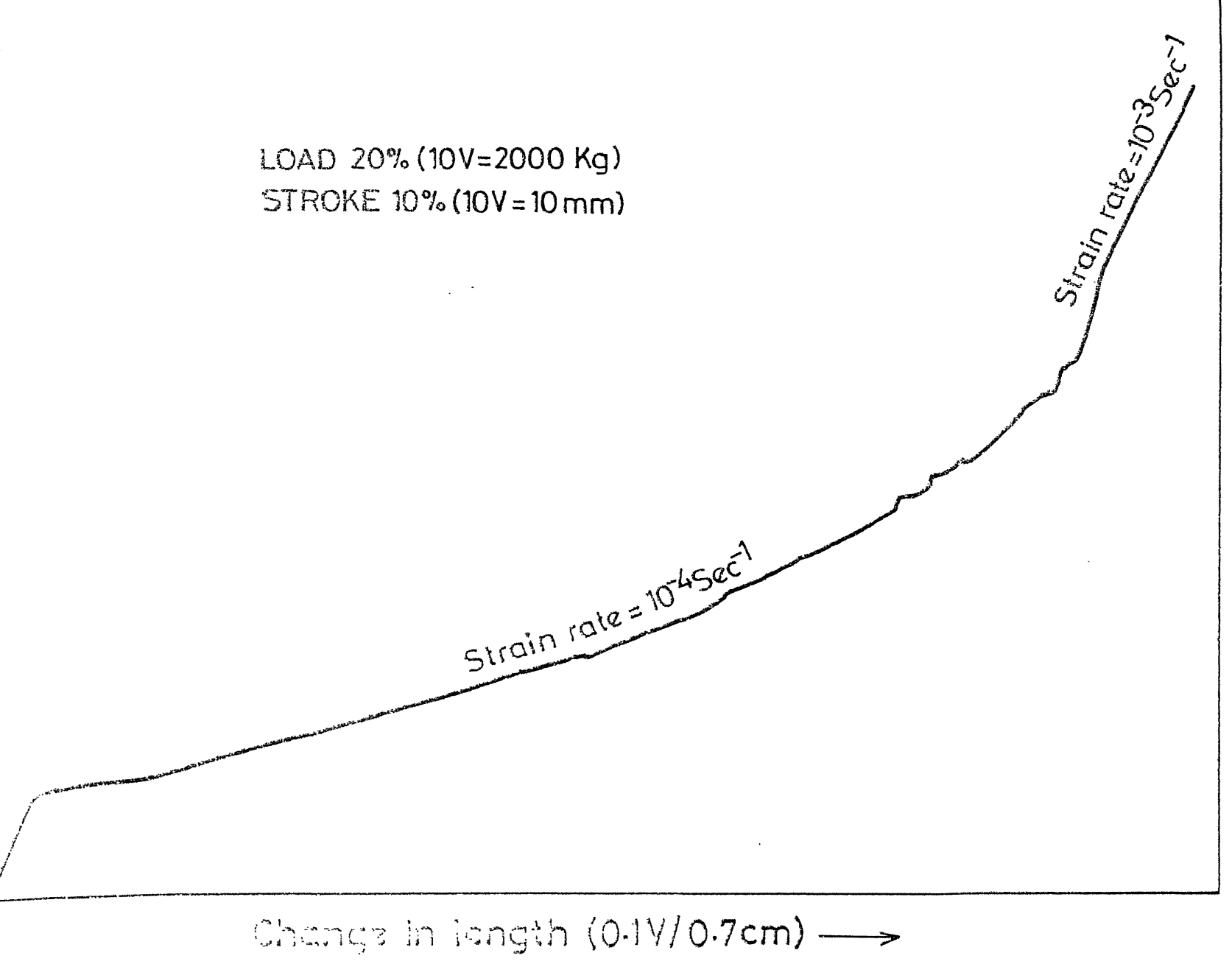

Fig. 4.8 Load vs change in length plot for pure NiAl.

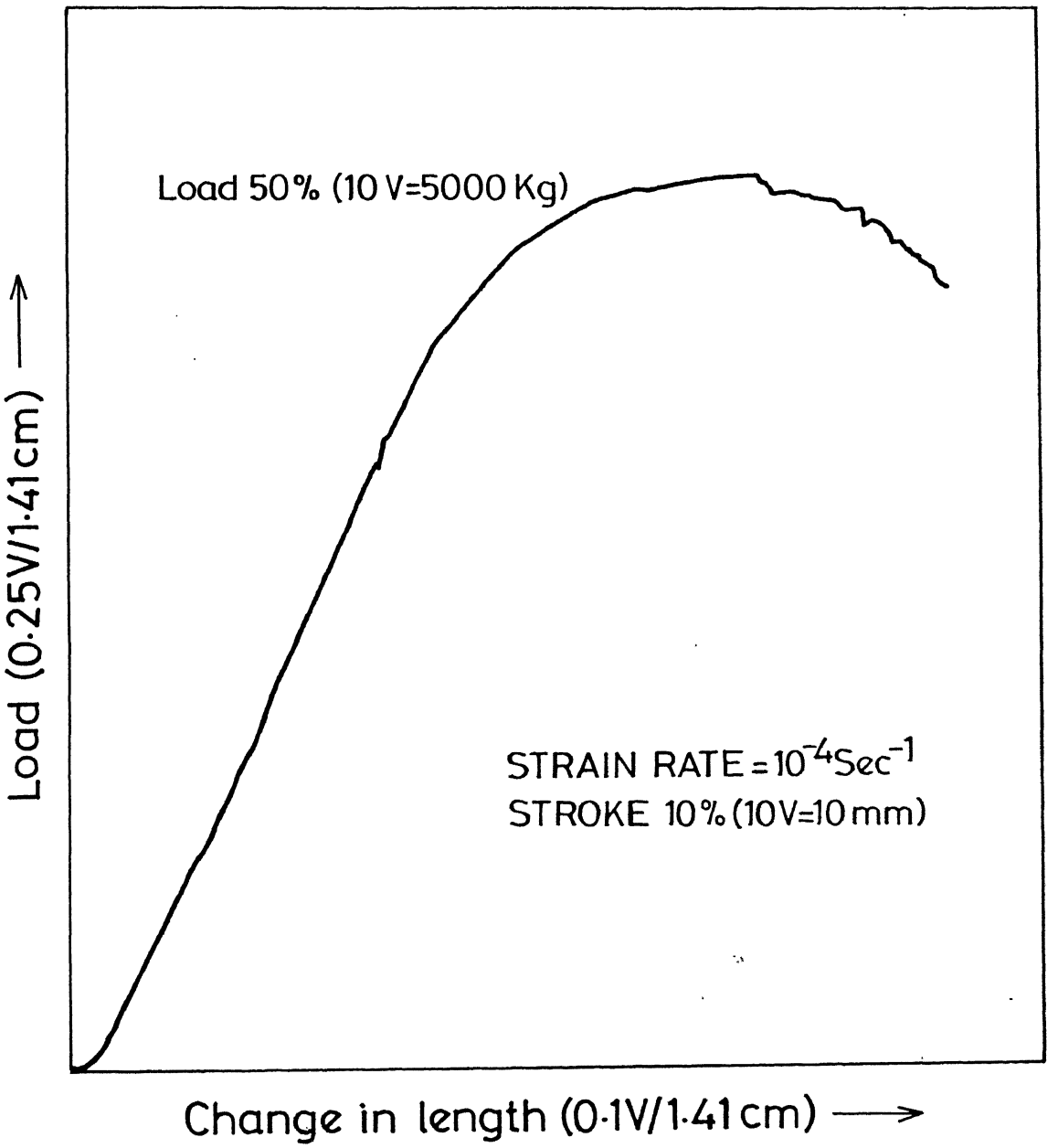

Fig. 4.14 Load vs change in length plot for 50 at.% Ni, 1.0 at.% Ta alloy.

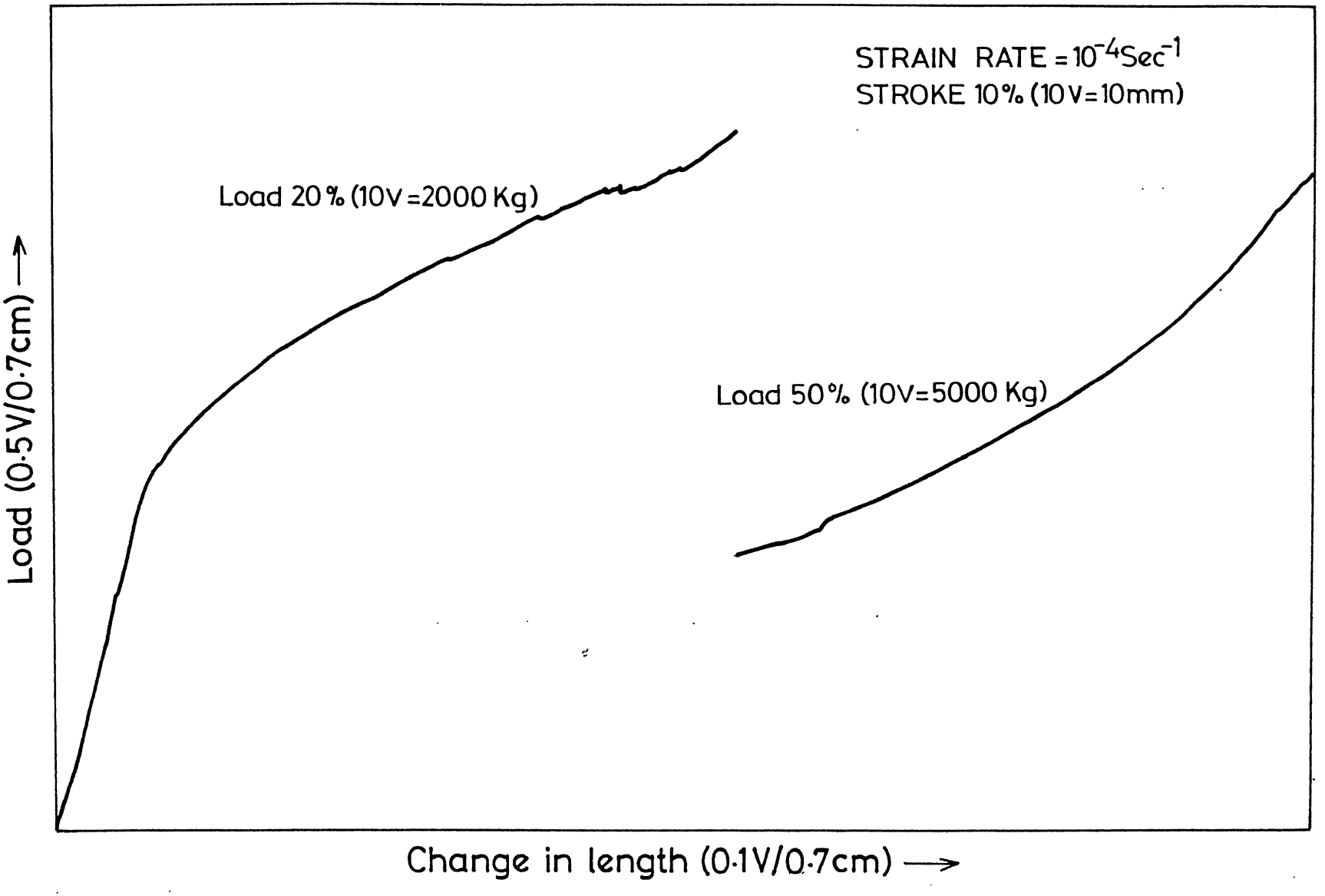

Fig. 4·20 Load vs change in length plot for 50 at.% Ni, 1·0 at.% Ta with B alloy.

Table 4.12 : Flow Stresses of Alloys

Alloy Composition			Flow Stress (MN/mm^2)	Percentage change in length	Remarks
at%Ni	at%Ta	Containing boron			
50	0	No	166.8	Greater than 50%	Sample did not fail and it become a disc
50	1.0	No	683.63	6% at the fracture stress	Sample failed due to brittle fracture
50	1.0	Yes	631.30	Greater than 68%	Sample did not fail and it become a disc while it was broken from corners

Fig 4.21: Photomicrograph of pure NiAl after compression,100X

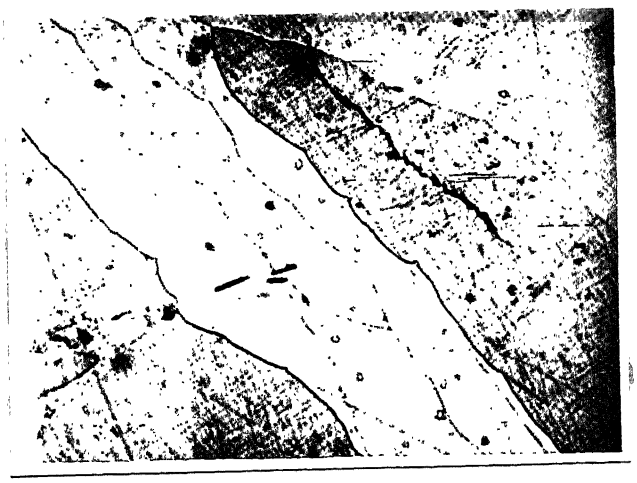

Fig 4.22: Photomicrograph of 50 at% Ni, 1.0 at% Ta alloy after compression , 100X

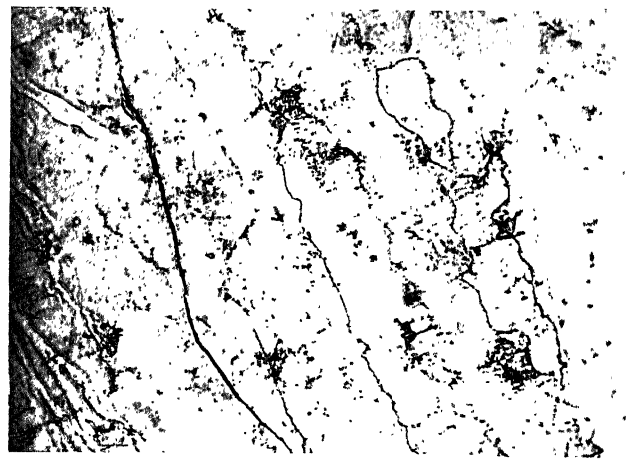

Fig 4.23: Photomicrograph of 50 at% Ni, 1.0 at% [illegible] compressing,100X

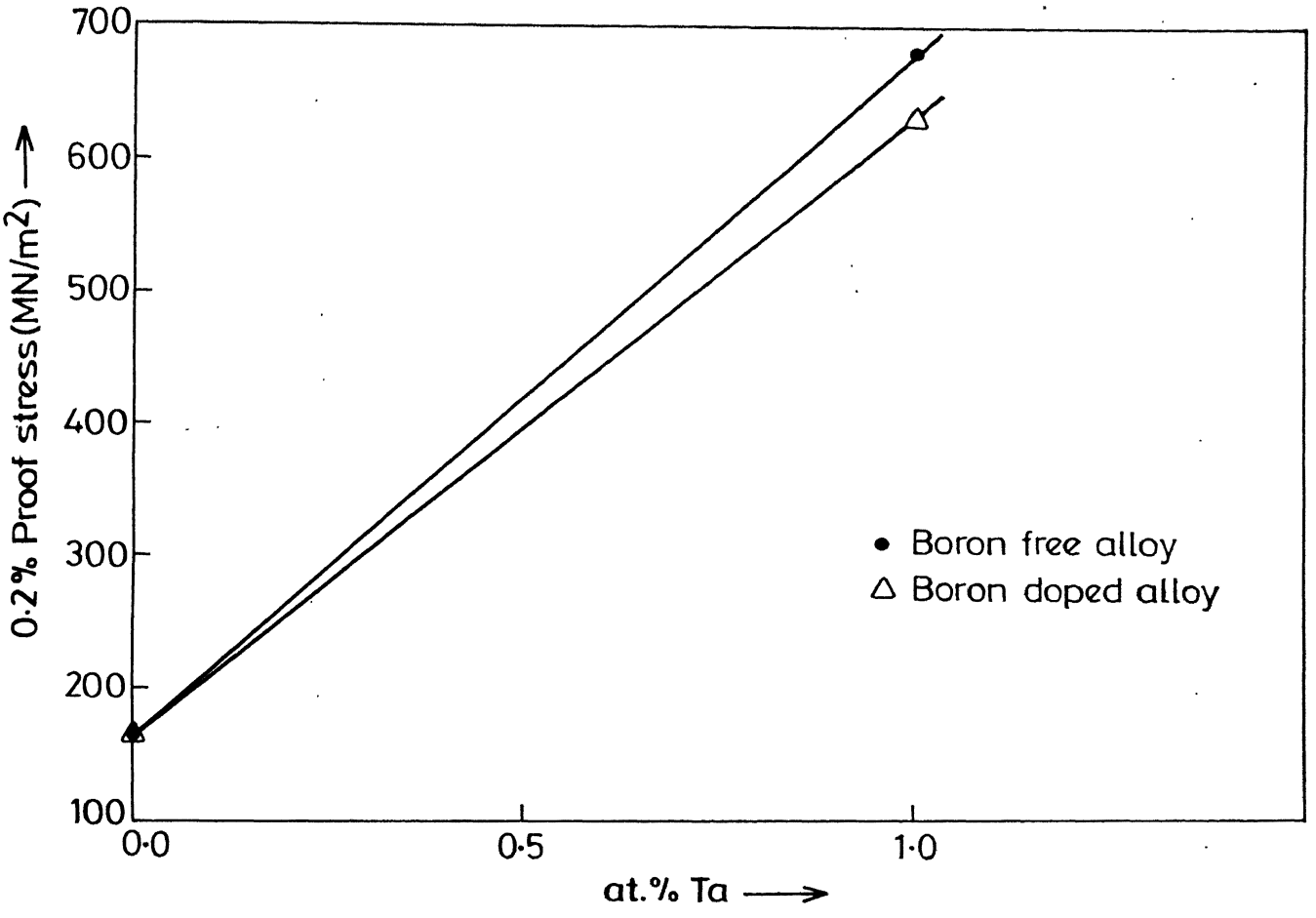

Fig. 4.24 0·2% Proof stress vs Composition plot.

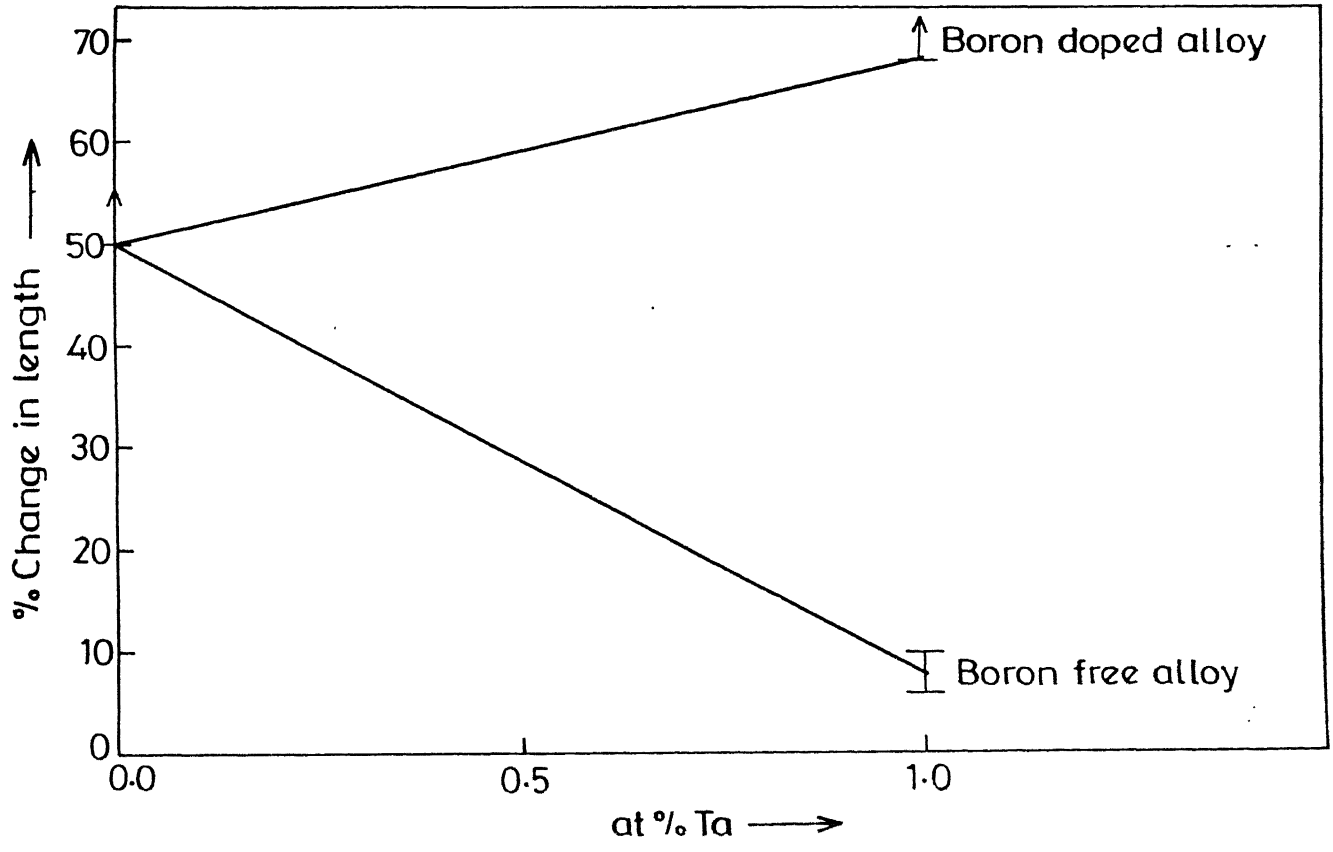

CHAPTER 5

DISCUSSION

5.1 Identification of Additional Diffraction Peaks

In order to identify the extra diffraction peaks which have been listed in last section in Tables (4.6) & (4.7) The diffraction peaks of intermetallic compounds expected to be present in the alloys have been taken from literature and listed in Table (5.1) and (5.2). Tables list the peaks due to Ni_3Al, Ni_2AlTa, Ni_6AlTa , Ni_3Ta, NiAlTa, TaC and Ni_3B.

Comparison of extra phase peaks found in 50 at% Ni, 0.6 at% Ta alloy free from boron. Contain particles of TaC at 1200^{o}C as well as at 1000^{o}C. 50 at% Ni, 1.0 at% Ta alloy free from boron also contain TaC particles. TaC particles are also found in 63.5 at% Ni, 1.5 at% Ta at 1000^{o}C and 50 Ni, 1.0 at% Ta-B at 1200^{o}C. The second phase particles in 50at% Ni, 0.6at% Ta-B are likely to be Ni_3B as the extra peaks match best with those of Ni_3B. A number of additional peaks present in other alloys could not be identified because of very small number of lines which were available. The above results have been summarised in Table (5.3).

Table 5.1 : Three Highest Intensity Peaks Values given in ASTM Index Card

	Ni_2AlTa (53)			Ni_6AlTa (54)			Ni_3Ta (55) Monoclinic			Ni_3Ta (56) Tetragonal			Ni_3Ta (57) Orthorhombic		
2θ	43.07	25.89	51.02	46.32	43.29	29.38	44.18	48.14	42.86	42.86	72.7	88.98	46.07	43.07	45.5
I/I_o	100	70	20	100	50	30	100	80	70	100	80	80	100	70	70

Table 5.2 : Diffraction Peak Values given in ASTM Index Card

NiAlTa (58)		TaC (59)		Ni_3Al (60)		Ni_3B (61)	
2θ	I/I_o	2θ	I/I_o	2θ	I/I_o	2θ	I/I_o
20.75	15	34.91	100	24.72	40	38.333	100
36.22	75	40.44	70	35.23	40	40.25	60
39.85	100	58.40	50	43.64	100	42.62	80
42.90	100	70.24	40	50.746	70	44.17	60
65.038	50	74.06	20	57.488	40	44.86	60
67.47	100	87.97	20	63.69	20	46.02	80
69.70	100	98.18	20	75.09	60	47.00	80
73.99	100			91.30	60	48.97	60
76.805	100			96.66	40	68.08	40
81.16	100					85.09	50

Table 5.3 : Phases Present in the Alloys

Alloy Compositions			Annealed at 1200°C	Annealed at 1000°C
at%Ni	at%Ta	Containing Boron		
50	0.6	No	Ni (Al, Ta) Small amount of TaC	Ni (Al, Ta) Lots of TaC
50	1.0	No	Ni (Al, Ta)	Ni (Al, Ta) Lots of TaC
50	5.0	No	Ni (Al, Ta) Additional phase (unidentified)	Ni (Al, Ta) Additional phase I (unidentified) Additional phase II (unidentified)
50	0.6	Yes	Ni (Al,Ta)with B	Ni(AlTaB)with B Ni_3B
50	1.0	Yes	Ni (AlTa) with B TaC	Ni(AlTa) with B
63.5	1.5	No	Ni(AlTa) Ni_3Al	Ni(Al,Ta) Ni_3Al TaC

5.2 Phase Diagram

The information given in Table (5.3) is plotted in Figure (5.1). The results obtained with the present investigation agree very well these reported in literature out of two sets of results available in the literature. The results of Nash and West (12) are more accurate then the others. The results of present investigation show that Ta does not replace Al in NiAl.

It is likely to replace both Ni as well as Al. It is indicated by solubility loop which tends to move towards Ni-rich end. On the basis of earlier data, one would have expected a symmetrical solubility loop where as the present investigation shows that loop is definitely asymmetric.

The solubility does not appear to change appreciately with temperature or boron content because 50 at% Ni, 1.0 at% Ta-B alloy at 1000^{o}C was single phase.

Many of the alloys contain TaC. Some altogether are free from carbides. Although the percentage of carbides is very small and each of carbon could be nickel as two batches of Ni of purity 99.9% and 99.99% had been used. The lower purity Ni may have contributed to carbon.

It appears that the solubility of TaC decreases rapidly with temperature. For example, 50 at% Ni, 1.0 at% Ta

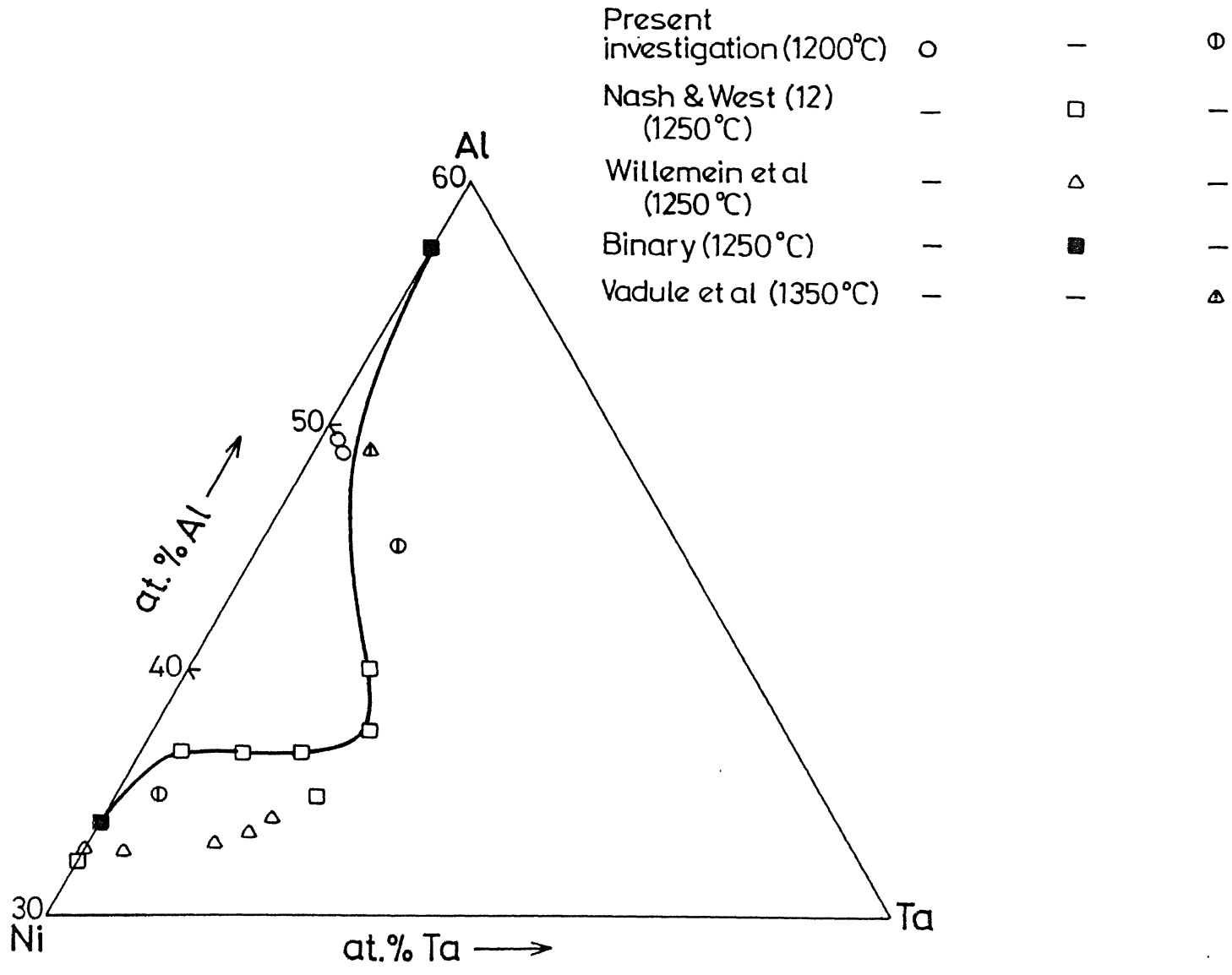

Fig. 5·1 Solubility of Ta in NiAl at 1250°C.

alloy is free from TaC carbon at 1200°C and contain lots of carbide particles at 1000°C. Many other alloys show similar behaviour.

5.3 Lattice Parameters

Lattice parameters of NiAl containing 50 at% Ni and Ta are plotted in Figures (5.2) and (5.3). Lattice parameters of NiAl-Ta have not measured. However, results suggest an slight decrease in lattice parameter at 1200°C with Ta content. It has been explained in previous section that Ta replaces both Al and Ni atoms. Ta of being higher atomic radius (1.46 Å than nickel (atomic radius = 1.26 Å), it can not occupy the nickel positions and create vacancies. Therefore, there is a decrease in lattice parameter occur. Lattice parameter of boron free alloys at 1000°C decrease drastically. This could not be explained because of two phase structures of both alloys 50at% Ni, 0.6 at% Ta and 50 at% Ni, 1.0 at% Ta at 1000°C. Presence of boron tends to increase the lattice parameter of NiAl. No such information is available in NiAl. However, boron tends to increase the lattice parameters of Ni_3Al (62). It is predicted that boron occupy the interstitial positions due to which lattice parameter increases.

5.4 Hardening

Microhardness of NiAl annealed at 1200°C is only 533 kg/mm^2 (52). Table of microhardness values given

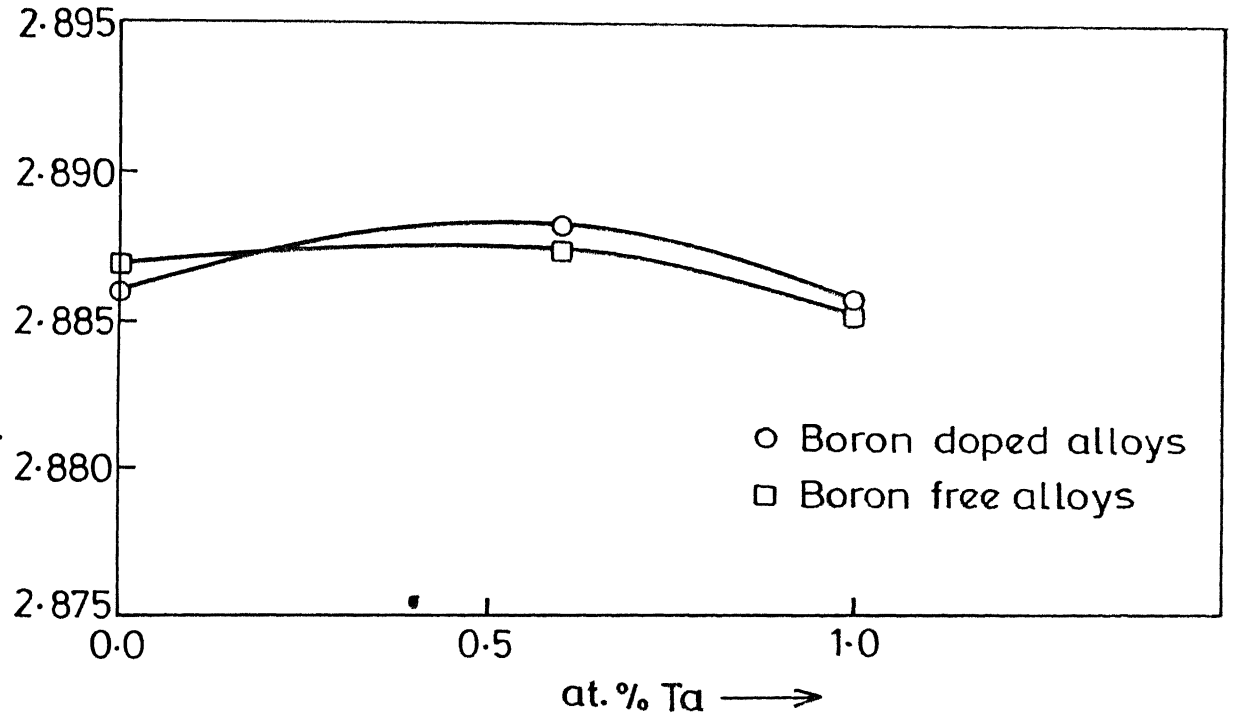

g. 5·2 Lattice parameter vs composition plots at 1200 °C.

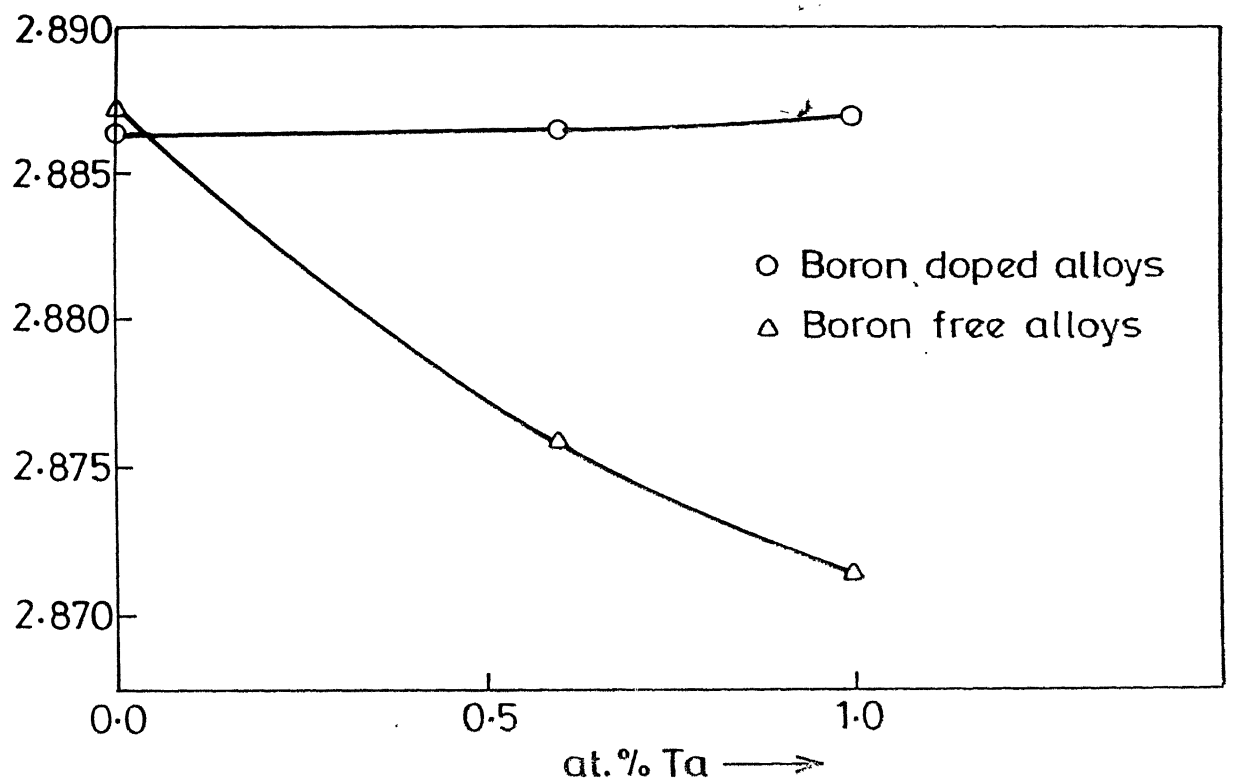

g. 5·3 Lattice parameter vs composition plots at 1000 °C.

earlier show that effect of Ta is appreciable in increasing the hardness. In presence of boron the hardening effect is further increased. Hardness is decreased at 1000^{o}C. This could be attributed to the removal of Ta by carbide formation.

5.5 Mechanical Properties under Compression

Lead versus change in length curve given in Figures 4.18, 4.19 and 4.20 show a typical behaviour. The values of 0.2% proof stress and percentage change in length reported earlier in Table (4.12). Plots of proof stress and % change in length versus composition are shown in Figure (4.24) and Figure (4.25) respectively. Ta tends to increase the flow stress considerably from 166.8 kg/mm^2 to 683.63 kg/mm^2. That is an increase of about 300% for only 1.0 at% of Ta. Boron has slight tendency to decrease the proof stress.

Pure NiAl is found to be quite ductile and it is possible to compress it in a thin disc. After adding 1 at% Ta fracture occur after 6 % change in length. However, presence of boron increases the ductility which becomes comparable with that of NiAl.

The microstructural examination showed that cracks in NiAl present in grain boundaries as well as through the grains in the presence of Ta cracks are mainly on grain

boundaries. However, in the presence of boron cracks propagated primarily through the grains.

Lots of recrystallization was observed in compressed samples. Recrystallisation observed primarily around the cracks. Suggesting that considerable stress concentration must have occur at crack tips. Boron seems to increase tendency of recrystallization.

Stress strain behaviour of intermetallic compounds may be expressed by equation

$$\sigma = K \varepsilon^n \qquad (5.1)$$

where n is work hardening coefficient and K is strength coeffic: Figure (5.4), Figure (5.5) and Figure (5.6) show the ln true stress versus ln true strain plots for pure NiAl, 50at% Ni, 1.0 at% Ta and 50 at% Ni, 1.0 at% Ta with B respectively. Slope is the value of n and value of K is obtained by value of ln σ at ε= 1. Values of K and n are listed in Table (5.4).

Table shows that K value increases by 175% by addition of Ta and around 200% by addition of boron and Ta. However, the work hardening coefficient tend to decrease with addition of B and Ta.

So these results suggest that addition of 1.0at% Ta and boron to NiAl are going to be extremely beneficial as they impart considerable increase in strength and appreciable ductility.

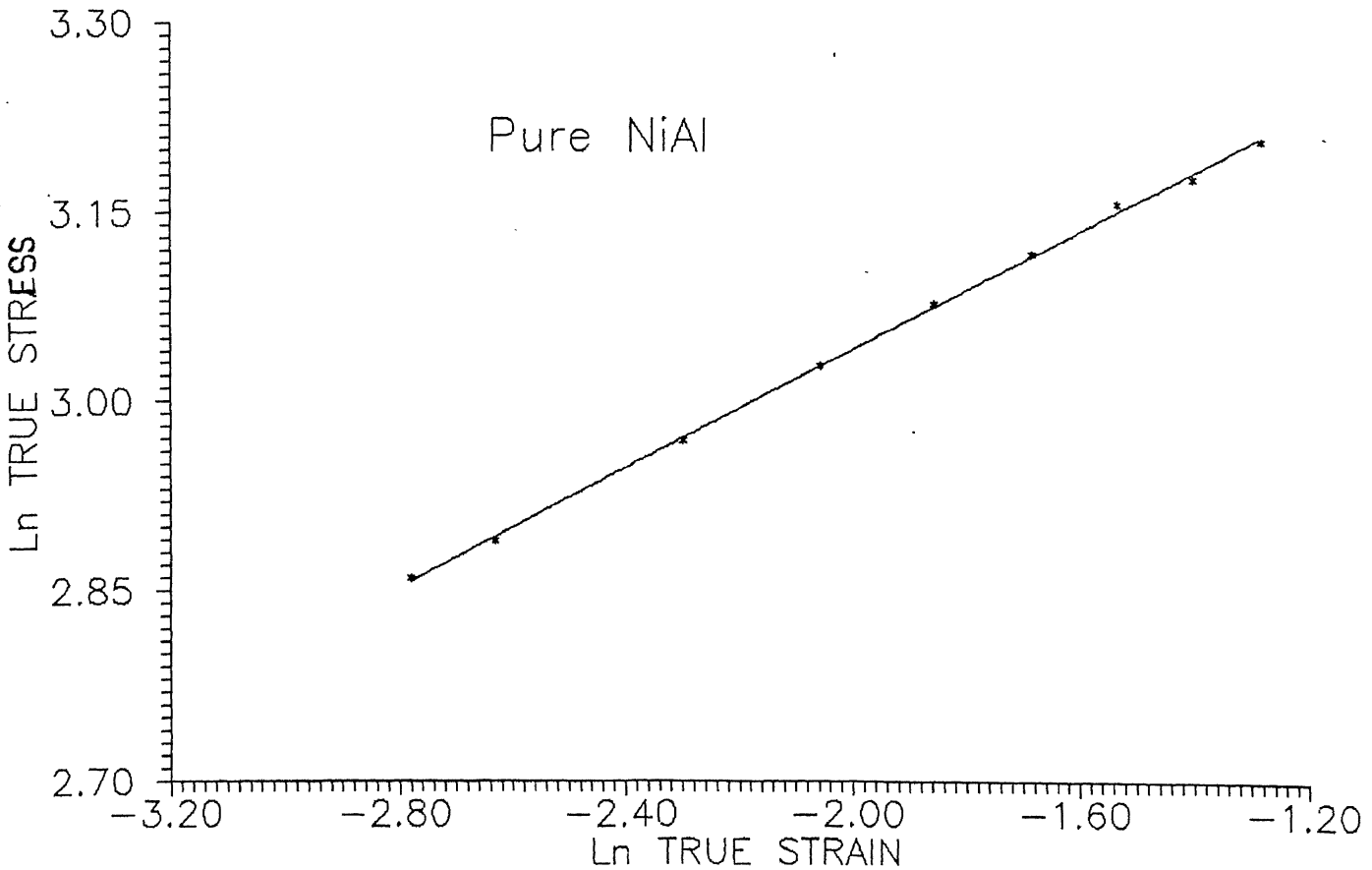

Fig 5.4: Ln True Stress vs Ln True Strain plot

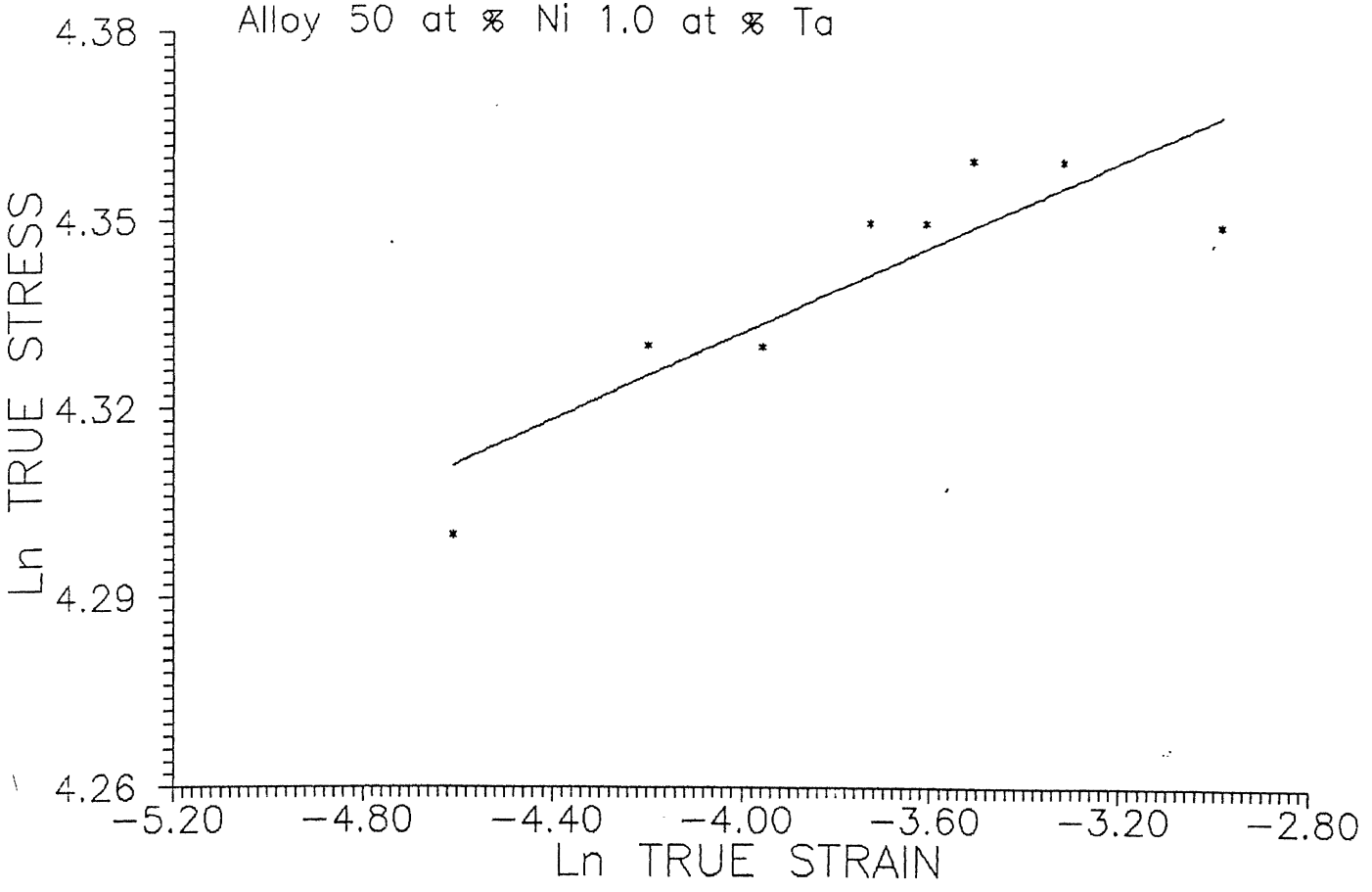

Fig 5.5 : Ln True Stress vs Ln True Strain plot

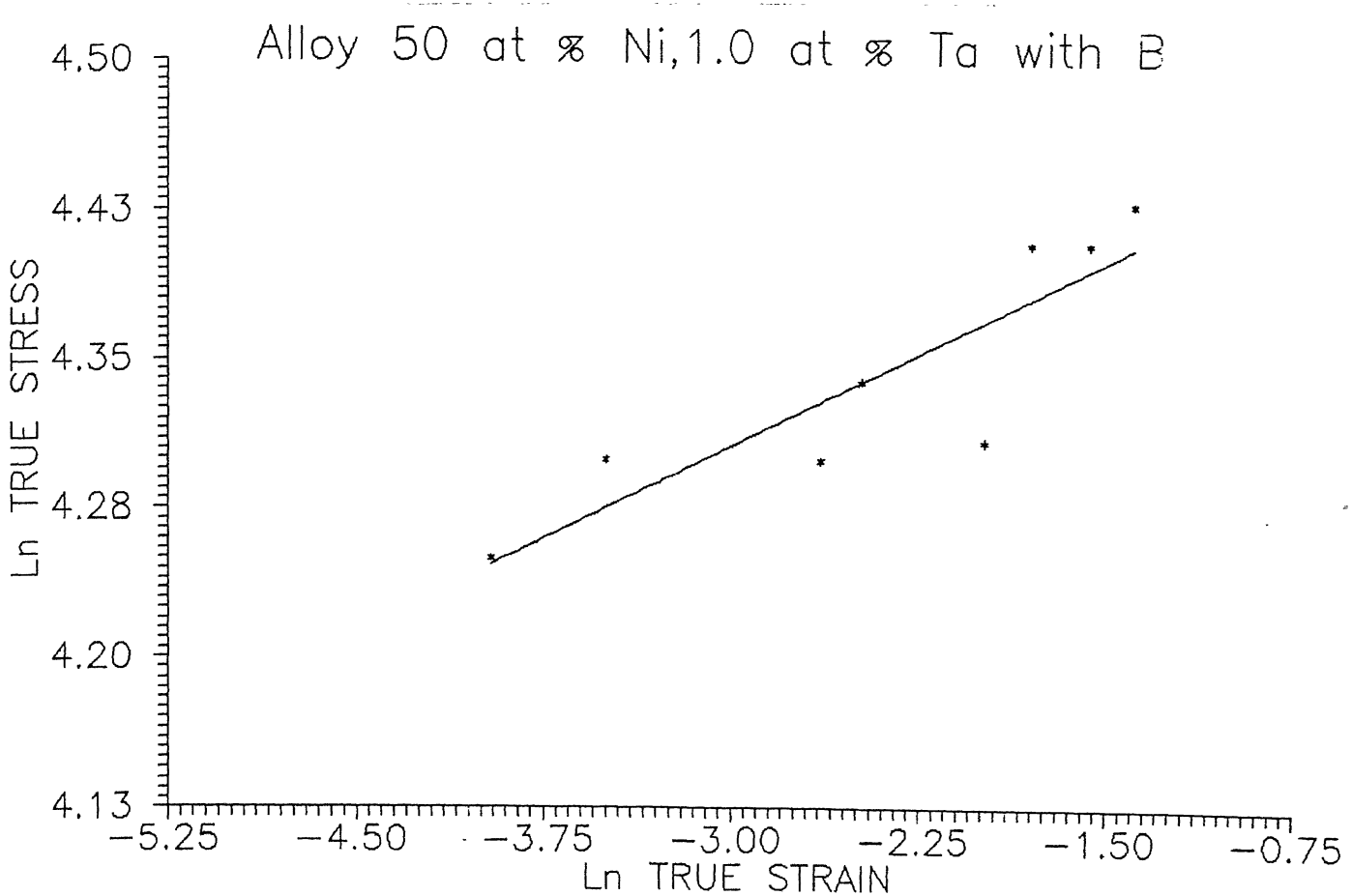

Fig 5.6: Ln True Stress vs Ln True Strain plot

Table 5.4 : K and n Values of Alloys at 550°C and Strain Rate 10^{-4} sec^{-1}

Alloy Composition			K(MN/m^2)	n
at%Ni	at%Ta	Containing boron		
50	0	No	331	.24
50	1.0	No	856.09	.035
50	1.0	Yes	882.16	.062

CHAPTER 6

SUMMARY AND CONCLUSIONS

(1) All alloys were homogenised at 1200°C and further equilibriated at 1000°C.

(2) These alloys were examined by X-ray diffraction and optical microscopy along with microhardness measurement of NiAl phase. Compression testing of pure NiAl, 50at% Ni, 1.0 at% Ta and 50 at% Ni, 1.0 at% Ta with B was also done.

(3) The results show that solubility of Ta in NiAl at 50 at% Ni is of the 1 at% and the solubility loop is asymmetric, suggesting the substitution of both Ni and Al. Also the literature value of Nash and West (12) appears to be more accurate than Willemein et al (17).

(4) Ta tends to decrease the lattice parameter of NiAl while boron tends to increase the lattice parameter.

(5) High temperature compression suggests that the presence of Ta increases the 0.2% proof stress but decreases the ductility. But in presence of boron and Ta, the strength is increased by more than 200% while ductility remains as high as of pure NiAl. Boron tends to prevent crack from propagating along the grain boundaries.

(6) Some amount of carbides were present in small volume fraction. Their effects have been ignored.

REFERENCES

(1) E.F. Bradley, 'Superalloys', ASM International Metals Park, OH 44073, 1988.

(2) E.W. Ross and C.T. Sims, 'Superalloy II', John Wiley and Sons, New York, 1987, pp. 97-133.

(3) M. Hansen and K. Anderko, 'Constitution of binary alloys', 1958, New York, McGraw Hill.

(4) M.J. Cooper, Phil. Maz. 84, pp. 805 (1963).

(5) F.A. Shunk, 'Constitution of binary alloys', 2nd supplement, 1959, New York, McGraw Hill.

(6) P. Nash and D.R.F. West, Met. Sci., 1983, 17, 99-100.

(7) J.H. Larson, R. Taggort and D.H. Polonis, 'Metall Trans.', 1970, 1, 485-489.

(8) E. Therkelsin, Met. Alloys, Vol. 4, 1933, pp. 105-108.

(9) A. Nash and P.Nash, 'Bulletin of Alloys Phase Diagram', Vol. 5, No.3, 1984, pp. 259-265.

(10) Eliot, 'Constitution of binary alloys', Ist Suppl. 1961, McGraw Hill.

(11) I. Edshammar and Holmberg, Acta Chem. Scand., 14, pp. 1219-1220 (1960).

(12) P. Nash and D.R.F. West, Met. Science, 1979, 13, 670-676.

(13) F. Mollard, B. Lux and J.C. Hubert, Z. Metall. Kd, 1974, 65, 461-468.

(14) B.C. Giessen and N.J. Grant, Acta Crystallography, 18, 1080 (1965).

(15) R.S. Mints et al., Sov. Fiz. Dok, 1973, 17, pp. 904-906.

(16) I.I. Kornilov, 'Intermetallic Compound', pp. 349-373, John Wiley and Sons, New York, 1969.

(17) P. Willemin, O. Durgue, M. Durrand-Clarre and J.H.Paridsen, 'Met. Sci. and Tech.', Vol. 12, 1986, pp. 34..

(18) P. Willemin, O. Dugue, M. Durrand-Charre and J.H. Davidson, 'Superalloys 1984', 637-647, 1984, Warrendala.Pa, The Metallurgical Society of AIME.

(19) K.M. Vedula, V.M. Pathre, I. Aslanidis and R.H. Titran, 'High Temperature Ordered Intermetallic Alloys', 39, p. 411, ed. C.C. Koch, C.T. Lin and N.S. Stotoff, Pittsburgh (1985).

(20) J.B. Kusma and H. Nawotny, Montash Chem., 18, 1080 (1965).

(21) W. Heine and V. Zwicker, Nantre Wiss, 49, 391 (1962).

(22) V. Pathare, G.M. Michal and K. Vedula, Scripta Metallurgica, Vol. 21, pp. 283-288, 1987.

(23) A.J. Bradley and A. Taylor, Proc. Roy. Society A (1937), 159, 56.

(24) L.N. Guseva, Doklady Akad. Nauk, S.S.S.R., 77, 415 (1951).

(25) H. Lipson and A. Taylor, Proc. Roy Society, A173, 232 (1939).

(26) A.E. Berkowitz, F.E. Joumot and F.C. Nix, Phys. Rev., 95, 1185 (1954).

(27) G.F. Hancock and B.R. Macdonell, Phys. Stat. Solidi (19), 4, 143 (1971).

(28) R.J. Wasilwski and J.E. Hauton, J. Phys. Chem. Solids, 30, 1929 (1969).

(29) R.J. Wasilwski, J. Phys. Chem. Solids, 29, 39 (1968).

(30) E.W. Elock and C.W. McComble, Phys. Rev., 109, 605 (1958).

(31) E.W. Elock, Proc. Phys. Soc., 73, 250 (1959).

(32) P.A. Flynn and G.M. Macmanus, Phys. Rev. 124, 59 (1961).

(33) E.M. Grala, "Mechanical Properties of Intermetallik Compound', edited by J.H. Westbrook, Wiley, New York (1960), p. 358.

(34) R.T. Passoe, K.C. Radford, R.D. Rawlings and C.W.A. Newey, J. Sci. Instruments, 1967, 44, 366.

(35) J.H. Holloman, Trans. Amer. Inst. Min. Met. Engg., 1945, p.162.

(36) L.P. Lautenchlager, D.A. Kiewit and J.O. Brittain, Trans. Met. Soc. AIME, 233, 1297 (1965).

(37) A. Ball and R.E. Smallman, Acta Metallurgica, 14, 1349 (1966).

(38) R.T. Pascoe and C.W.A. Newey, Met. Sci. J, 2, 138 (1968).

(39) W.J. Yang and R.A. Dodd, Met. Sci. J, 7, 41 (1973).

(40) J.D. Whittenberger, J. of Mat. Sci. 22, pp. 394 (1987).

(41) S. Shankar and L.L. Siegle, Met. Trans. 9A, 1467 (1978).

(42) O.D. Sherby, R.H. Klundt and A.K. Miller, Met. Trans., 8A, 843 (1977).

(43) A. Ball, Ph.D. Thesis, Univ. of Brimingham (1964).

(44) E.M. Schulson, Res. Mech. Letters, 1, 111, (1981).

(45) E.M. Schulson and D.R. Barker, Scripta, Metallurgica, Vol. 17, 519 (1983).

(46) R. Van Mises, Z. Angew. Math. Mech, 8, 161 (1928).

(47) R.R. Vandervoort, A.K. Mukherjee and J.E. Doon, Trans. ASM, 59, 930 (1966).

(48) I. Backer and P.R. Munroe, Journal of Metals, Vol. 2, p. 28, 1988.

(49) A. Inone, T. Masumoto and H. Tornioka, Journal of Materials Science, 19, p. 3097, (1984).

(50) C.C. Law and M.J. Blackburn, 'Rapidly Solidified Light Weight Durable Disk Material', (Report FR-18674-4, Pratt and Whitney Group 1985).

(51) A.H. Cottrell, Trans. Metall. Soc. AIME, 212, p. 192 (1958).

(52) Dr. H.K. Gupta, Department of Metallurgical Engineering, I.I.T. Kanpur.

(53) ASTM Index Card No. 30-31.

(54) ASTM Index Card No. 34-1284.

(55) ASTM Index Card No. 19-855.

(56) ASTM Index Card No. 18-893.

(57) ASTM Index Card No. 17-699.

(58) ASTM Index Card No. 18-45.

(59) ASTM Index Card No. 35-801.

(60) ASTM Index Card No. 9-97.

(61) ASTM Index Card No. 19 -834.

(62) Y.G. Kim, G.W. Yoon and N.S. Stoloff, J. of Mat. Sci., 4, (1985), 1407-1408.